Title
SUPERCONDUCTING QUANTUM INTERFERENCE DEVICES FOR LOW FREQUENCY MEASUREMENTS

Author
Clarke, John.

Publication Date
1976-06-01

Lecture given at the Nato Advanced Study Institute, Lago di Garda, Italy, September 1 - 10, 1976; also To be published as a Chapter in "Superconductor Applications: Squids and Machines" (1977), Brian B. Schwartz and Simon Foner, eds., Plenum Publishing Corporation

LBL-5192

SUPERCONDUCTING QUANTUM INTERFERENCE DEVICES FOR LOW FREQUENCY MEASUREMENTS

John Clarke

June 24, 1976

Prepared for the U. S. Energy Research and Development Administration under Contract W-7405-ENG-48

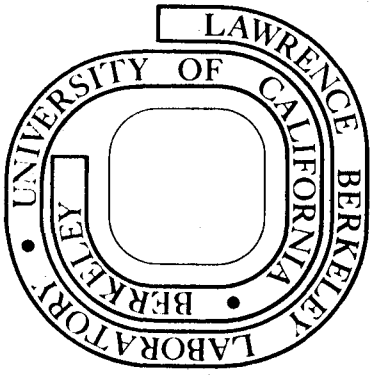

DISCLAIMER

Reprinted from: SUPERCONDUCTOR APPLICATIONS: SQUIDS AND MACHINES (1977)
Edited by Brian B. Schwartz and Simon Foner
Book available from Plenum Publishing Corporation
227 West 17th Street, New York, New York 10011

Chapter 3

SUPERCONDUCTING QUANTUM INTERFERENCE DEVICES FOR LOW FREQUENCY MEASUREMENTS

John Clarke

Department of Physics

University of California

Berkeley, California 94720

and

Materials and Molecular Research Division

Lawrence Berkeley Laboratory

Berkeley, California 94720

I. INTRODUCTION

Quantum interference effects between two Josephson tunnel junctions [1] incorporated in a superconducting ring were first observed by Jaklevic et al. [2] in 1964. These workers showed that the critical current of the double junction was an oscillatory function of the magnetic flux threading the ring, the period being the flux quantum, Φ_o. The implications of this result for instrumentation were quickly realized, and a variety of dc SQUIDS* (Superconducting Quantum Interference Devices) were developed and used. These devices included several designs involving machined pieces of niobium connected with point contact junctions [3-5], and the SLUG [6] (Superconducting Low-Inductance Undulatory Galvanometer), which consisted of a bead of solder frozen onto

*The prefix "dc" indicates that the device is operated with a direct current bias, while the prefix "rf" indicates that the device operates with an rf flux bias. The rf SQUID is mis-named, as no quantum interference takes place.

a niobium wire. In the late 1960's, the rf SQUID [7-9] appeared. The rf SQUID consists of a single Josephson junction on a superconducting ring, and, presumably because only a single junction is required, has become much more widely used than the dc SQUID. Several commercial versions [10-13] of the rf SQUID, complete with sophisticated readout electronics, are available. Close attention has been paid to the optimum coupling of the rf SQUID to the room temperature electronics. As a result of this research, the present rf SQUIDs have a higher sensitivity than the first generation of dc SQUIDs. However, Clarke, Goubau, and Ketchen [14] have recently described a thin-film tunnel-junction dc SQUID that is also ideally coupled to the room temperature electronics. The sensitivity of this dc SQUID is limited by its intrinsic noise and is one-to-two orders of mangitude higher than that of the earlier dc SQUIDs; it compares favorably with that of most rf SQUIDs.

In this article, I outline the principles and operation of both dc and rf SQUIDs, and describe their applications to low frequency measurements. The general outline follows that of an earlier review [15]. Section II very briefly reviews the relevant facts of flux quantization and Josephson tunneling, and mentions the important practical configurations of Josephson junctions. Sections III and IV are concerned with the dc SQUID and the rf SQUID respectively. In each section I have used the same parallel development: Theory, operation, noise theory, fabrication and performance, and future improvements. Section V is devoted to applications of dc and rf SQUIDs. I describe first the principles of the flux transformer, and then discuss in turn magnetometers, gradiometers, susceptometers, and voltmeters, mentioning the principles involved, indicating where improvement in performance is needed, and comparing the SQUID-based devices with alternative instruments. Finally, in Section VI, I mention some of the practical applications in which SQUIDs have been used or in which they have potential use.

II. SUPERCONDUCTIVITY AND THE JOSEPHSON EFFECTS

In a superconductor, some of the free electrons are paired together [16]. These Cooper pairs are in a macroscopic quantum state that can be described by a single wavefunction [17]

$$\psi(\vec{r}, t) = |\psi(\vec{r}, t)| \exp[i\phi(\vec{r}, t)] \quad ,$$

where $|\psi|$ and ϕ are the amplitude and phase of the wavefunction. The existence of this macroscopic quantum state gives rise to several observable phenomena, for example, flux quantization [17, 18] and Josephson tunneling [1].

A. Flux Quantization

The requirement that ψ be single-valued at any point in a closed superconducting ring is expressed by the Bohr-Sommerfeld condition

$$\oint \vec{p} \cdot d\vec{s} = \oint 2m\vec{v} \cdot d\vec{s} + \oint 2e\vec{A} \cdot d\vec{s} = nh \quad . \tag{1}$$

In Eq. (1), $\vec{p} = 2m\vec{v} + 2e\vec{A}$ is the pair canonical momentum, m and e are the electron mass and charge, $\vec{v}$ is the pair-velocity, $\vec{A}$ is the vector potential, $d\vec{s}$ is an element of length, h is Planck's constant, and n is an integer. The term $\vec{v}$ is proportional to the supercurrent flowing around the ring in a penetration depth λ. Provided that the thickness of the ring is much larger than λ, we may choose the path of integration in a region of zero current, so that $\oint \vec{v} \cdot d\vec{s} = 0$. The term $\oint \vec{A} \cdot d\vec{s} = \int \mathrm{curl} \vec{A} \cdot d\vec{S} = \vec{B} \cdot d\vec{S}$ ($\vec{B}$ is the magnetic field and $d\vec{S}$ is a surface element) is just the total magnetic flux Φ in the ring, which in general consists of an applied flux and a screening flux generated by induced supercurrents. Equation (1) then reduces to the condition

$$\Phi = nh/2e = n\Phi_o \quad . \tag{2}$$

Thus the flux contained in the ring is quantized in units of the flux quantum $\Phi_o = h/2e \approx 2 \times 10^{-15}$ Wb.

B. The Josephson Equations

The "classical" Josephson [1] tunnel junction consists of two superconducting films separated by a thin insulating barrier. If zero current flows through the junction, the superconductors are coupled by an energy [1, 19, 20]

$$E_c = -I_c \Phi_o / 2\pi \quad . \tag{3}$$

Provided that $|E_c| \gg k_B T$, the phases of the two superconductors are locked together, and a time-independent supercurrent can be passed through the barrier up to a maximum value of I_c, the critical current. The difference between the phases of the two superconductors, θ, adjusts to the externally applied current I according to

$$I = I_c \sin\theta \quad . \tag{4}$$

If a current greater than I_c is passed through the junction, a voltage V appears across it, and the supercurrent oscillates at a frequency

$$\nu = (1/2\pi)\, d\theta/dt = 2eV/h = V/\Phi_o \quad . \tag{5}$$

C. Types of Josephson Junctions and their Current-Voltage Characteristics

There are three main types of junctions that are currently used in SQUIDs. The first is the tunnel junction [20] (Fig. 1(a)), which is fabricated by evaporating or sputtering a strip of superconductor onto an insulating substrate, oxidizing the strip thermally or by a glow discharge in oxygen, and depositing a second strip of superconductor. Early tunnel junctions

were not very reliable, and alternative weak-link configurations were consequently developed and used in devices. However, in the past few years, very reproducible and reliable tunnel junctions have been produced. The most useful junctions appear to be Pb - PbOx - Pb [21-24], Nb - NbOx - Pb [25], and Nb - NbOx - Nb [26]. All of these junctions can be stored at room temperature and recycled many times without significan deterioration, and appear to be less prone to damage from electrical transients than some other types of weak link. Their critical currents have very little temperature dependence below 4.2K. Photoresist techniques [27] have been used to produce evaporated lead strips with widths down to about 1 μm.

Josephson tunnel junctions exhibit hysteresis in their I-V characteristic, as shown in Fig. 1(b). For most SQUID applications, it is essential that the I-V characteristic by non-hysteretic. The hysteresis may be removed (Fig. 1(c)) by shunting the junction with a resistance R such that the hysteresis parameter [28]

$$\beta_c = 2\pi I_c R^2 C/\Phi_o \leqslant 1 \quad , \tag{6}$$

where C is the junction capacitance (typically 2 pF for a 10 x 10 μm junction). The shunt may consist either of a small disk of normal metal that underlays the intersection of the two superconductors, or of a diagonal normal strip joining the two superconductors near their intersection [29].

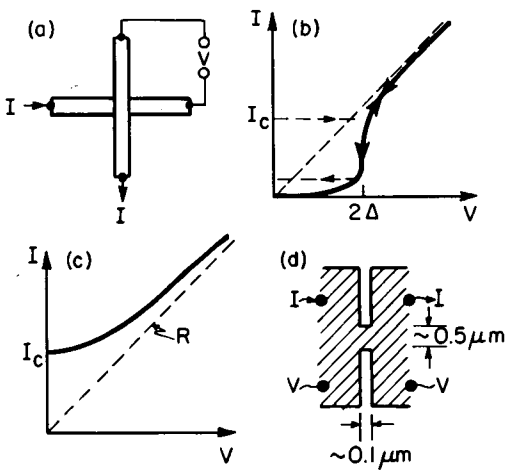

Fig. 1. (a) Josephson tunnel junction; (b) I-V characteristic of Josephson tunnel junction with identical superconductors (Δ is the energy gap); (c) I-V characteristic of shunted Josephson junction ($\beta_c \ll 1$); (d) Anderson-Dayem bridge.

In the latter case, the junction and the strip must be covered with an insulating layer (too thick to permit tunneling) and a superconducting ground plane to reduce the stray inductance to a negligible level. If $\beta_c \ll 1$, the I-V characteristic is described (in the absence of noise) by [28]

$$V = R\left(I^2 - I_c^2\right)^{1/2} \quad . \tag{7}$$

From Eq. (7) we can immediately obtain the dynamic resistance

$$R_D = R / [1 - (I_c / I)^2]^{1/2} \quad . \tag{8}$$

The second kind of commonly used Josephson junction is the Anerson-Dayem [30] bridge shown in Fig. 1(d). In this structure, there is no tunneling barrier, but rather a superconducting "weak link" connecting two superconducting films. The most reliable bridges are probably those fabricated from niobium [31-33], $NbSe_2$ [34], or Nb_3Ge [35]. In one version, the bridge is "weakened" by a thin normal metal underlay or overlay [8,31].

The third widely used junction is the point contact [36]. Its properties have been reviewed extensively by Zimmerman [37]. The point contact junction consists essentially of a sharpened niobium point pressed against a niobium block. In some versions, the pressure of the contact can be changed by means of a differential screw operated from outside the cryostat. Versions that can be recycled repeatedly without adjustment have also been developed [38].

In point contacts that are clean (non-oxidized), and in bridges whose length is long compared with a coherence length, deviations [39] from the ideal sinusoidal current-phase relation [Eq. (4)] are to be expected. The voltage-frequency relation is always exact. In this article, we shall always assume a sinusoidal current-phase relation. Deviations from this behavior do not affect the principles on which the SQUIDs operate, but may give rise to substantially higher intrinsic noise [40].

III. DC SQUID

A. Theory of the dc SQUID

The dc SQUID consists of two Josephson junctions mounted on a superconducting ring (Fig. 2). When the external flux threading the ring, Φ_e, is changed monotonically the critical current of the two junctions oscillates as a function of Φ_e, with a period Φ_o. At low voltages, the voltage across the junctions at constant bias current is also periodic in Φ_e. Semi-quantitative descriptions of this behavior have been given by De Waele and R. de Bruyn Ouboter [41] and by Tinkham [42]. We will sketch the more recent numerical calculation by Tesche and Clarke [43].

We derive a set of equations describing the time-dependent behavior of the SQUID. The inductance of the ring is L, and the critical

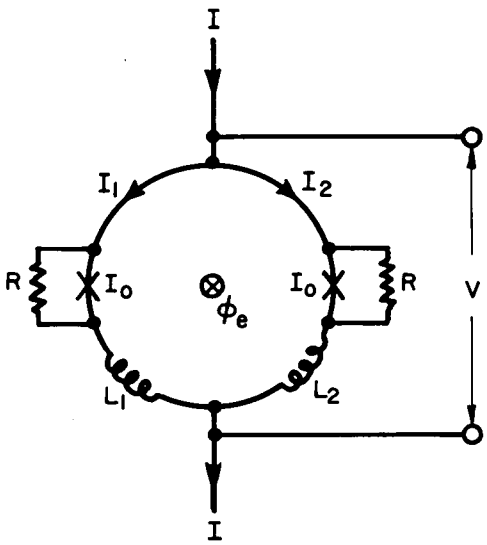

Fig. 2. Configuration of dc SQUID

current and shunt resistance of each junction are I_c and R. The SQUID is biased with a constant current I, and the currents through the two junctions are $I_1(t)$ and $I_2(t)$. Thus

$$I = I_1 + I_2 \quad . \tag{9}$$

We define a circulating current $J(t)$ as

$$J = (I_2 - I_1)/2 \quad . \tag{10}$$

The currents $I_1(t)$ and $I_2(t)$ are related to the voltages $V_1(t)$ and $V_2(t)$ and phase differences $\theta_1(t)$ and $\theta_2(t)$ across the junctions by

$$I_1 = I_c \sin\theta_1 + V_1/R \quad , \tag{11}$$

and

$$I_2 = I_c \sin\theta_2 + V_2/R \quad , \tag{12}$$

where

$$d\theta_1/dt = (2e/\hbar)\, V_1 \quad , \tag{13}$$

and

$$d\theta_2/dt = (2e/\hbar)\, V_2 \quad . \tag{14}$$

The total voltage V developed across the SQUID is

$$V = V_1 + L_1 dI_1/dt + M dI_2/dt \tag{15}$$

$$= V_2 + L_2 dI_2/dt + M dI_1/dt , \tag{16}$$

where L_1 and L_2 are the self-inductances of the two arms of the SQUID, and M is the mutual inductance between the arms.

The phase differences θ_1 and θ_2 are related by

$$\theta_1 - \theta_2 = 2\pi\Phi_T/\Phi_o , \tag{17}$$

where Φ_T is the total flux in the SQUID. The total flux is the sum of the individual fluxes Φ_1 and Φ_2 produced by the currents I_1 and I_2 and the external quasistatic flux Φ_e. (Because the SQUID responses are periodic in Φ_e with period Φ_o, we make the restriction $0 \le \Phi_e \le \Phi_o$.) If we define $\ell_1 = -\Phi_1/I_1$ and $\ell_2 = -\Phi_2/I_2$ we can easily show that $\ell_1 + \ell_2 = L$; we take the symmetric case $\ell_1 = \ell_2 = L/2$. The flux produced by the currents I_1 and I_2 is thus $-LI_1/2 + LI_2/2 = LJ$, and the total flux is just

$$\Phi_T = \Phi_e + LJ . \tag{18}$$

The quantities L, L_1, L_2, ℓ_1, ℓ_2, and M are related in the following way. Suppose that in some time-dependent mode $dI_1/dt \neq 0$ while $dI_2/dt = 0$. The inductive voltage drop around the ring (neglecting any contributions from the junctions) is $V = L_1 dI_1/dt - M dI_1/dt$. The rate of change of flux in the ring yields $V = \ell_1 dI_1/dt$. Hence $\ell_1 = L_1 - M$, and, similarly, $\ell_2 = L_2 - M$. Using these expressions for M and the fact that $dJ/dt = -dI_1/dt = dI_2/dt$ (since I is constant), we can reduce Eqs. (15) and (16) to

$$V = V_1 - (L/2)\, dJ/dt \tag{19}$$

$$= V_2 + (L/2)\, dJ/dt . \tag{20}$$

These equations include the effect of the mutual inductance even though M does not appear explicitly.

We define $\beta = 2LI_c/\Phi_o$. The final set of equations can be derived from Eqs. (9) to (20). Hence, from Eqs. (17) and (18)

$$\frac{J}{I_c} = \frac{\theta_1 - \theta_2}{\pi\beta} - \frac{2\Phi_e}{\beta\Phi_o} ; \tag{21}$$

from Eqs. (13), (17), and (19)

$$V = \frac{\hbar}{4e}\left(\frac{d\theta_1}{dt} + \frac{d\theta_2}{dt}\right) ; \tag{22}$$

and from Eqs. (9) to (14),

$$\frac{d\theta_1}{dt} = \frac{2eR}{\hbar}[(I/2) - J - I_c \sin\theta_1], \tag{23}$$

and

$$\frac{d\theta_2}{dt} = \frac{2eR}{\hbar}[(I/2) + J - I_c \sin\theta_2]. \tag{24}$$

These equations can be solved numerically to find all the characteristics of the dc SQUID (for details of the methods of solution, see Tesche and Clarke [43]). In Fig. 3 we plot the critical current I_m of the SQUID as a function of Φ_e for several values of the parameter $\beta = 2LI_c/\Phi_o$. I_m is periodic in Φ_e with period Φ_o. Notice that the curve is smooth near $\Phi_e = 0$ and Φ_o, and cusped at $\Phi_e = \Phi_o/2$. In the limit of large β, the maximum change in critical current, ΔI_m, approaches Φ_o/L; for $\beta = 1$ (a typical value for practical SQUIDs), ΔI_m is approximately $\Phi_o/2L$. In Fig. 4 we plot I-V characteristics with $\Phi_e = \Phi_o/2$ for $\beta \sim \infty$, 2.0, 1.0, and 0.4. As $\beta \to \infty$, the relative critical current modulation depth $\Delta I_m/2I_m \to 0$; this curve is thus identical with the curves for lower values of β with $\Phi_e = 0$. For $\beta = 1$, as Φ_e is changed from 0 to $\Phi_o/2$, we observe a modification of the I-V characteristic that is considerable at low voltages, but that progressively decreases as the voltage (or bias current) is increased. This decrease can be understood in the following way. The circulating current, J(t), has a maximum value at $\Phi_e = \Phi_o/2$ and oscillates at a frequency that increases as the voltage across the SQUID is increased. When this frequency becomes comparable with R/L, a further increase in the bias current causes the amplitude of J(t) to decrease, and hence the modfication of the I-V characteristic at $\Phi_e = \Phi_o/2$ also decreases.

This effect is also shown in Fig. 5, where we plot the average voltage across the SQUID as a function of Φ_e for several values of bias current and with $\beta = 1$. The decrease in the voltage modulation amplitude ΔV with increasing bias current is clearly demonstrated. Notice also that the cusp in the I_m vs Φ_e curve at $\Phi_e = \Phi_o/2$ is rounded out in the V vs Φ_e curve.

As we shall see later, the important parameter when the SQUID is used as a device is $(\partial V/\partial \Phi_e)_I$. Values of $(\partial V/\partial \Phi_e)_I$ may be deduced from Fig. 5. However, an order-of-magnitude estimate can be obtained as follows. The voltage modulation depth (the change in voltage when Φ_e is changed from $n\Phi_o$ to $(n + 1/2)\Phi_o$) for a SQUID with $\beta \approx 1$ is just

$$\Delta V \approx r_D \Delta I_m \approx r_D \Phi_o / 2L \quad . \tag{25}$$

In Eq. (25), r_D ($= R_D/2$) is the dynamic resistance of the two junctions in parallel. If $r_D \approx 1\,\Omega$ and $L \approx 10^{-9}$ H, we find $\Delta V \approx 1\,\mu$V. From Eq. (25) we find

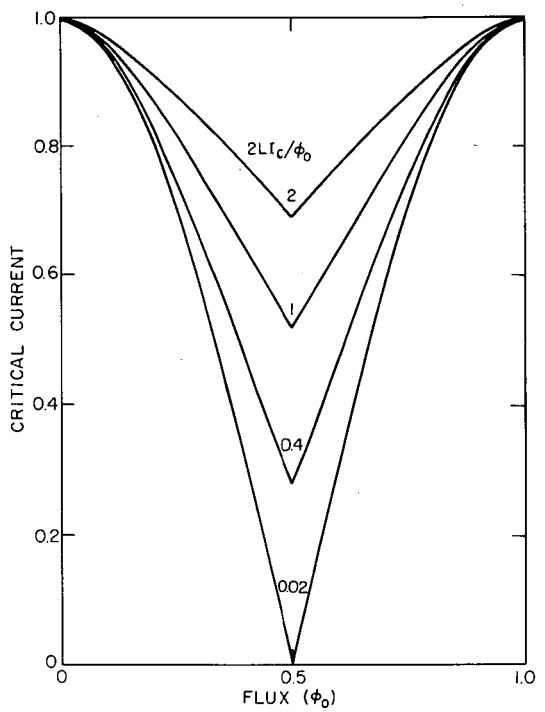

Fig. 3. Reduced critical current vs applied flux for four values of $\beta = 2LI_c/\Phi_o$.

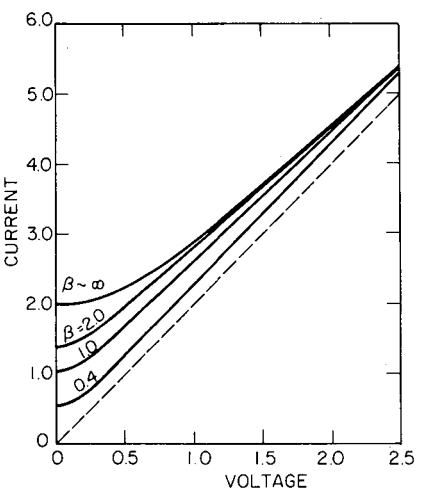

Fig. 4. Current (in units of $2I_c$) vs. voltage (in units of I_cR) for a dc SQUID for four values of $\beta = 2LI_c/\Phi_o$.

$$\left(\frac{\partial V}{\partial \Phi_e}\right)_I \approx \frac{r}{L} \quad , \tag{26}$$

about $2\mu V \Phi_o^{-1}$. Here, r is the parallel resistance of the two shunts; we have set $r_D \approx r$.

B. Operation of the dc SQUID

To detect changes in the flux threading the dc SQUID, we bias the SQUID at a nonzero voltage with a steady current, I_o, and apply a sinusoidal modulation flux of peak-to-peak amplitude $\sim \Phi_o/2$ and frequency f = 100 kHz. This flux is generated by passing a current in the modulation coil that is mounted inside the SQUID. As illustrated in Fig. 6(a), the ac voltage across the SQUID has a large component at 2f and zero component at f when $\Phi_e = (n + 1/2)\Phi_o$. As Φ_e is increased from $(n+1/2)\Phi_o$, the amplitude V_f of the ac signal across the SQUID at the fundamental frequency f increases (initially linearly), while the component at 2f decreases. The f component reaches a maximum at $\Phi_e = (n+3/4)\Phi_o$ (Fig. 6(b)), and becomes zero again when $\Phi_e = (n+1)\Phi_o$; it reverses phase at $\Phi_e = n\Phi_o$ and $(n+1/2)\Phi_o$. Figure 6(c) shows the variation of V_f with Φ_e near $(n+1/2)\Phi_o$. Although the exact value of $(\partial V_f/\partial \Phi_e)_{I_o}$ near $(n+1/2)\Phi_o$ depends on the detailed shape of the V vs Φ_e curve, a reasonable estimate is $\sim 2\Delta V/\Phi_o$.

The ac voltage across the SQUID is amplified by room temperature electronics, and lock-in detected at frequency f, as shown in Fig. 7. The lock-in detector produces an output that is proportional to the amplitude of the signal across the SQUID at frequency f. The output from the lock-in is integrated. Thus, with the feedback loop open, the quasistatic output from the integrator is periodic in Φ_e (provided that the gain of the broadband amplifier in Fig. 7 is reduced almost to zero: otherwise the lock-in and integrator will saturate). When the feedback switch is closed, the output from the integrator is connected via a resistor R_F to the modulation coil. The feedback system maintains the total flux in the SQUID near either $n\Phi_o$ or $(n+1/2)\Phi_o$, depending on the sign of the feedback. This configuration is known as the flux-locked SQUID. When the flux applied to the SQUID is changed by $\delta\Phi_e$, a current is fed back into the modulation coil that produces an opposing flux $-\delta\Phi_e$. Thus the SQUID is always operated at a constant flux and serves as a null detector in a feedback circuit. The voltage developed across R_F is proportional to $\delta\Phi_e$.

The ac-modulation and lock-in detection together with the negative feedback minimize certain sources of drift and 1/f noise, for example: changes in the critical current caused by changes in the bath temperature; drifts in the bias current, I_o; drifts in the thermal emf's in the cryostat leads; and 1/f noise in the preamplifier.

A major difficulty in the past has been the satisfactory coupling of the dc SQUID to the room temperature electronics. At 100 kHz, a state-of-the-art low noise FET preamplifier has an optimum noise temperature of about 1 K for a source impedance of about 100 kΩ.

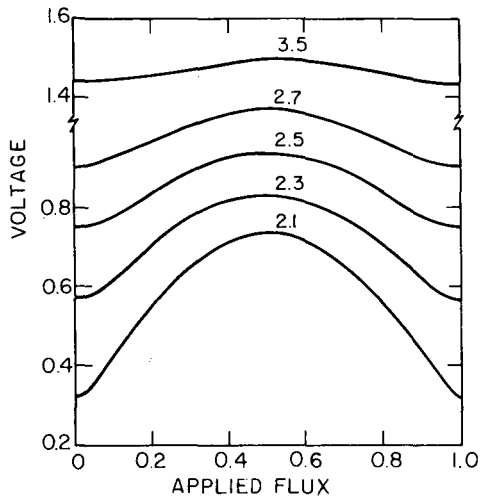

Fig. 5. SQUID voltage (in units of $I_c R$) vs. applied flux (in units of Φ_o) for $I_o/2I_c = 2.1$, 2.3, 2.5, 2.7, and 3.5.

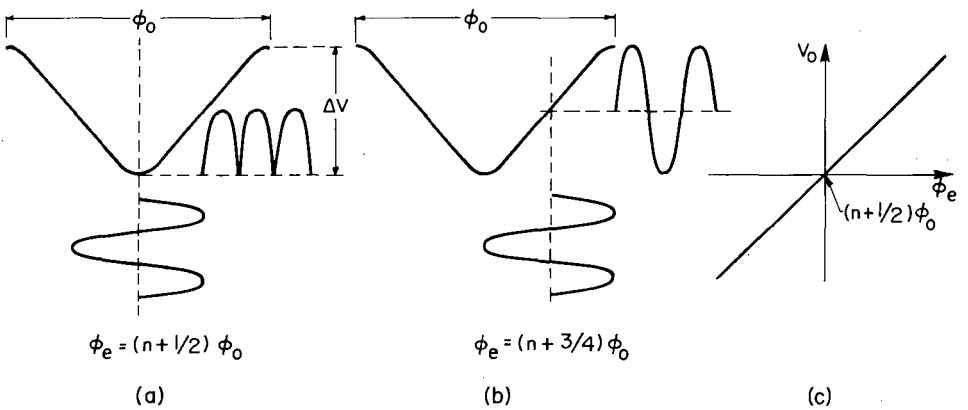

Fig. 6. Voltages across SQUID produced by an ac modulating flux of frequency f. In (a) $\Phi_e = (n+1/2)\,\Phi_o$; in (b) $\Phi_e = (n+3/4)\,\Phi_o$; the amplitude of the output voltage at f as a function of Φ_e is shown in (c) for Φ_e close to $\Phi_o/2$.

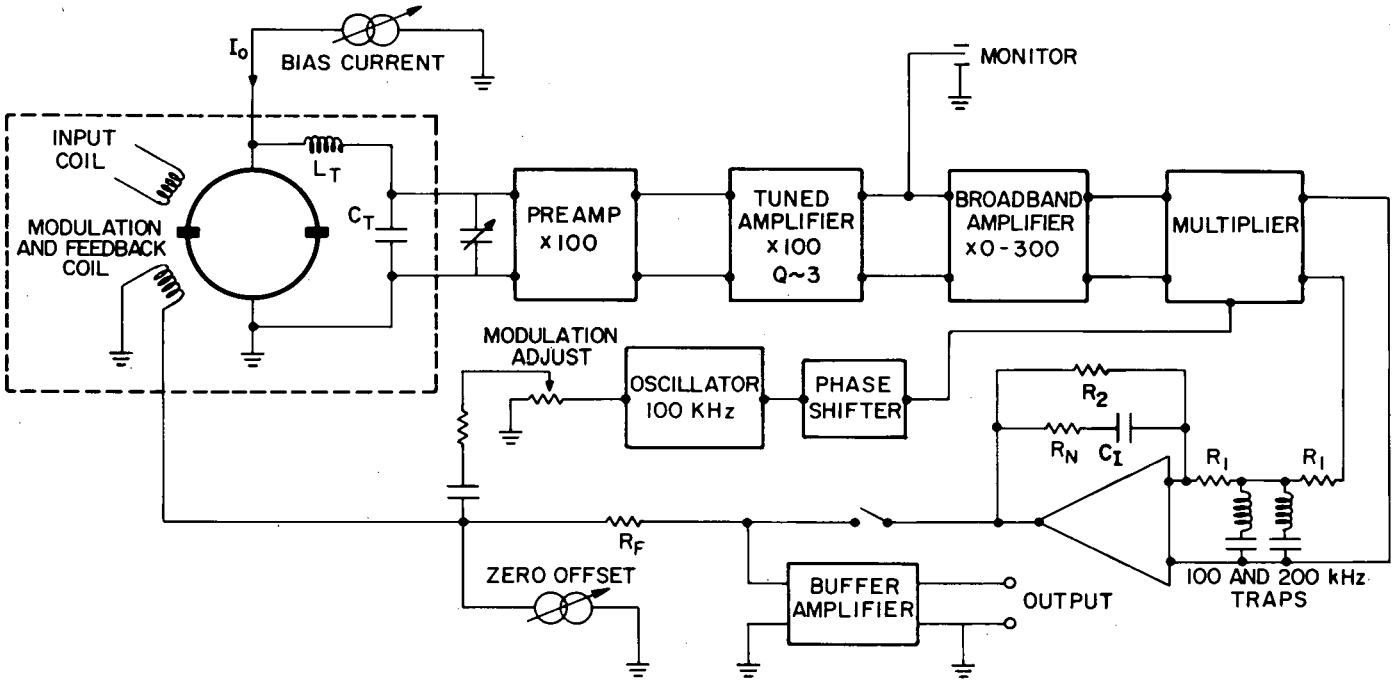

Fig. 7. Schematic of dc SQUID electronics. Components within the dashed box are at liquid helium temperature.

Therefore, it is necessary to enhance the ac impedance of the SQUID ($\sim 1\Omega$) by a factor of about 10^5 to achieve optimum low noise performance. Clarke et al. [14] achieved satisfactory impedance matching by means of a cooled LC circuit resonant at 100 kHz, as shown in Fig. 7. The tank circuit amplifies the signal by $Q \sim 150$, and amplifies the SQUID impedance by $Q^2 \sim 2 \times 10^4$.

A rough estimate of the amplitude of the signal obtained from the tank circuit can be made in the following way. Suppose an ac flux of peak-to-peak value $\Phi_o/2$ is applied to the SQUID with $\Phi_e = (n \pm 1/4)\Phi_o$. A 100 kHz voltage of peak-to-peak amplitude $\sim r_D \Phi_o / 2L$ appears across the SQUID. The tank circuit amplifies this signal by an amount $Q = \omega L_T / r_D$, provided that r_D is the dominant resistance in the tank circuit (L_T is the inductance, and $\omega = 2\pi f$). The peak-to-peak signal across the tank circuit is then

$$V_T \approx \Phi_o \omega L_T / 2L \quad . \tag{27}$$

If $L_T \approx 200\,\mu H$, and $L \approx 1\,nH$, we find $V_T \approx 100\,\mu V$. When the SQUID is operated in the feedback mode, the parameter of interest is $(\partial V_T / \partial \Phi_e)_{I_o}$ near a turning point in the V vs Φ_e curve. Since V_T represents the peak-to-peak voltage for a peak-to-peak flux Φ_o, we have*

$$\left(\frac{\partial V_T}{\partial \Phi_e}\right)_{I_o} \approx \frac{\omega L_T}{L} \quad , \tag{28}$$

about $200\,\mu V\,\Phi_o^{-1}$ for the parameters gives above. It should be noted that $(\partial V_T / \partial \Phi_e)_{I_o}$ is independent of Q and r_D, provided that the losses in the tank circuit are dominated by dissipation in r_D.

C. Theory of Noise in the dc SQUID

We discuss first the white noise limitations due to intrinsic SQUID noise and preamplifier noise. To properly evaluate the performance of a SQUID, one must specify not only the rms flux noise as a function of frequency, but also the SQUID inductance and the coupling coefficient between the SQUID and input coil. These factors will be discussed at the end of this section.

A detailed analysis of the intrinsic white noise in a dc SQUID has recently been carried out by Tesche and Clarke [43]. They added two independent noise terms to Eqs. (11) and (12), each representing the

*If the V vs Φ_e curve is represented as a series of triangles, it can be shown [9, 14] that $(\partial V_T / \partial \Phi_e)_{I_o} = (8/\pi) V_T$. In view of the other approximations involved, we have neglected the factor $(4/\pi)$ in the present analysis.

Johnson noise in one of the resistive shunts, and used a digital computer to calculate the flux noise power spectrum as a function of various parameters. We shall give here an approximate analysis [14] that yields results within a factor of two of the numerical calculation.

Consider first a single shunted junction with $\beta_c = 0$. The I-V characteristic is "rounded" by Johnson noise in the shunt, the degree of rounding increasing as the parameter $\gamma = I_c\Phi_o/2\pi k_B T$ is decreased from ∞ ($T = 0$) to 0 ($I_c = 0$). The shape of the noise-rounded I-V characteristic has been calculated by Ivanchenko and Zil'berman [44], Ambegaokar and Halperin [45], and Vystavkin et al. [46]; these calculations are in good agreement with the experiments of Falco et al. [47]. Likharev and Semenov [48] and Vystavkin et al. [46] have calculated the noise power spectrum for a shunted junction. For frequencies much less than the Josephson frequency at the given voltage bias, they find a white voltage noise power spectrum

$$S_V = \left[1 + \frac{1}{2}\left(\frac{I_c}{I_o}\right)^2\right]\frac{4k_B T R_D^2}{R} \quad , \tag{29}$$

where R_D is the noise-rounded dynamic resistance. An inspection of the noise-rounded I-V characteristics [44-46] for $\gamma \approx 25$ (typical for our SQUIDs) and for $I/I_c \approx 1.3$ (typical operating bias), indicates that R_D is not substantially different from its value in the absence of noise [Eq. (8)]. We shall therefore use the noise-free value of R_D in Eq. (29) to obtain the voltage noise power spectrum.

The Johnson noise in the resistive shunts affects the dc SQUID in two ways: It induces a voltage noise across the SQUID, and it induces a circulating current noise that in turn generates a flux noise in the SQUID. A detailed analysis, however, indicates that the flux noise power is typically an order of magnitude smaller than the equivalent flux noise power due to the voltage noise, and we shall neglect the flux noise contribution.

Since the only dc SQUID on which detailed noise measurements have been made is that of Clarke et al. [14], we shall present a noise analysis in which a tank circuit is used to amplify signals from the SQUID. The analysis is readily adapted to SQUIDs connected directly to a preamplifier, or with transformer coupling. The voltage noise power spectrum referred to the output of the tank circuit is*

*This noise estimate is reasonably accurate when the SQUID is biased near a critical current maximum (i.e., $\Phi_e \approx n\Phi_o$). However, it is less accurate when the SQUID is biased near a minimum (i.e., $\Phi_e \approx (n+1/2)\Phi_o$), because the I-V characteristic is significantly distorted from the form of Eq. (7). However, it is thought that Eq. (30) is accurate to within a factor of about 2. A more exact numerical calculation appears in Ref. 43.

$$S_v^{(t)} \approx Q^2\left[1+\frac{1}{2}\left(\frac{I_m}{I_o}\right)^2\right]\frac{4k_BTr_D^2}{R} \approx \left[1+\frac{1}{2}\left(\frac{I_m}{I_o}\right)\right]^2\frac{4k_BT\omega^2L_T^2}{r}. \quad (30)$$

The total voltage noise power spectrum is the sum of $S_v^{(t)}$ and the preamplifier voltage noise power spectra $S_v^{(p)} + S_I^{(p)}Q^4r_D^2$. $S_v^{(p)}$ is the voltage noise power spectrum when the preamplifier input is shorted, while the second term represents the voltage generated by the preamplifier current noise flowing through a source resistance $Q^2 r_D$. The flux noise power spectrum of the SQUID is found be dividing twice* the total voltage noise power spectrum by $(\partial V_T/\partial \Phi_e)^2_{I_o}$:

$$S_\Phi = 2\left\{\left[1+\frac{1}{2}\left(\frac{I_m}{I_o}\right)^2\right]\frac{4k_BT\omega^2L_T^2}{r} + S_v^{(p)} + S_I^{(p)}\frac{\omega^4L_T^4}{r_D^2}\right\}\Bigg/\left(\frac{\partial V_T}{\partial \Phi_e}\right)^2_{I_o}. \quad (31)$$

Equation (31) indicates how S_Φ can be optimized. For a given SQUID, ac modulation frequency, and preamplifier, the only variable is L_T, which can be varied without affecting the resonant frequency by changing C appropriately. Since $(\partial V_T/\partial \Phi_e)^2_{I_o} \propto \omega^2L_T^2$, the contribution of the SQUID voltage noise term to S_Φ is independent of L_T, and the problem is reduced to one of choosing L_T to optimize $\left[\left(S_v^{(p)}/\omega^2L_T^2\right) + \left(S_I^{(p)}\omega^2L_T^2/r_D^2\right)\right]$. The optimum value is given by $S_v^{(p)}/S_I^{(p)} = Q^4r_D^2 = \omega^2L_T^4/r_D^2$. Since the noise temperature of a state-of-the-art FET preamplifier is about 1 K, the contribution of the preamplifier noise to S_Φ when the SQUID is operated at 4 K is almost negligible.

One very important consideration concerning the noise characterization of SQUIDs will be mentioned here, although it is equally applicable to both dc and rf SQUIDs. In almost all practical applications, the magnetic flux to be measured is coupled into the SQUID be means of a second superconducting coil that we shall refer to as the input coil (see Section V for examples). The relevant noise parameter then involves not only the flux noise of the SQUID, but also how efficiently the input

*The factor of 2 arises because of the effects of the 100 kHz modulation and lock-in detection scheme. Noise is mixed into the bandwidth around 100 kHz both from frequencies near zero, and from frequencies around 200 kHz. This calculation is carried through in detail in Appendix C of Ref. 14.

coil is coupled to the SQUID. Let the input coil of inductance* L_i have a mutual inductance M_i with the SQUID, where $M_i^2 = \alpha^2 L_i L$. Let the minimum detectable current change per $\sqrt{Hz}$ in the input coil be $\delta I_i = S_\Phi^{1/2}/M_i$. We then take as our figure of merit the energy per Hz associated with the current, $\varepsilon = L_i(\delta I_i)^2/2$, or

$$\varepsilon = S_\Phi L_i/2M_i^2 = S_\Phi/2\alpha^2 L \quad . \tag{32}$$

We see that ε represents the minimum energy resolution of the SQUID per Hz, $S_\Phi/2L$, multiplied by $1/\alpha^2$. This figure of merit, or a variation of it, has been used by a number of authors [9, 14, 15, 49-53]. It should be noted, however, that it is strictly valid only in the zero-frequency limit. As has been emphasized by Claassen [53], and as we shall see explicitly in Section V, this figure of merit is appropriate for all SQUID applications at low frequencies, and provides a meaningful way of comparing different SQUIDs. To optimize SQUID sensitivities, one should seek to minimize $S_\Phi/2\alpha^2 L$, rather than S_Φ. In practice, one usually determines ε by measuring S_Φ, L_i, and M_i. It is difficult to measure the parameters α and L separately, although $\alpha^2 L$ is of course known once L_i and M_i are determined.

Equation (32) can be used to express the intrinsic SQUID energy resolution in a particularly useful way. If we assume that the preamplifier noise is negligible, by using Eq. (28) with Eq. (31), we find

$$S_\Phi/2\alpha^2 L \approx 4k_B T/(r/L), \tag{33}$$

where we have neglected $(I_m/I_o)^2/2 \leq 1/2$. The energy resolution is thus $4k_B T$ divided by the characteristic frequency or "sampling frequency", of the SQUID, r/L.

D. Practical dc SQUIDs: Fabrication and Performance

The earliest practical dc SQUIDs were the point contact version of Zimmerman and Silver [36] (Fig. 8), and the SLUG [6]. The SQUID consisted of a split hollow niobium cylinder, with the two halves rigidly clamped together, but electrically insulated with mylar spacers. Two sharpened niobium screws in one half-cylinder could be adjusted to make point contact junctions with the other half-cylinder. Buhrman, Strait, and Webb [38] used thin sheets of glass expoxied to the niobium

---

*Note that, in general, the inductance of the input coil when it is coupled to the SQUID is lower than when it is free-standing. The reduction in inductance is a result of the ground-planing effect of the SQUID. Throughout this article, L_i refers to the inductance of the coil when it is coupled to the SQUID.

for electrical insulation. The thermal expansion coefficient of the glass was matched to that of the niobium, so that the SQUID could be thermally recycled. The most sophisticated (published) electronics for these early dc SQUIDs was that of Forgacs and Warnick [5], who achieved an rms flux resolution of about $10^{-3}\,\Phi_0\,Hz^{-1/2}$. This sensitivity seems to be typical of the early dc SQUIDs, and apparently was limited by preamplifier noise rather than intrinsic SQUID noise.

Relatively little development of the dc SQUID took place in the late 1960's and early 1970's, presumably because of the growing interest in the rf SQUID. However, there has recently been a revival of interest in the dc SQUID. Mercereau and coworkers [54, 55] and Richter and Albrect [56] have fabricated thin-film planar dc SQUIDS using Dayem bridges. Mercereau and colleagues used Nb, Nb_3Sn, and NbN thin films that are extremely stable under thermal cycling. Clarke, Goubau and Ketchen [14] developed the thin-film tunnel junction dc SQUID, and since this version appears to have the best performance, I shall discuss it in detail.

The substrate is a fused quartz tube 20 mm long with an outside diameter of 3 mm (Fig. 9). A band of Pb/In alloy (approximately by wt. 10% indium) about 11 mm wide and 3000 Å thick is evaporated around the tube. A 250 μm wide 750 Å thick gold film is then evaporated: this film is the shunt for the tunnel junctions. Next, two 150 μm wide 3000 Å thick niobium films, separated by 1.2 mm, are dc sputtered onto the

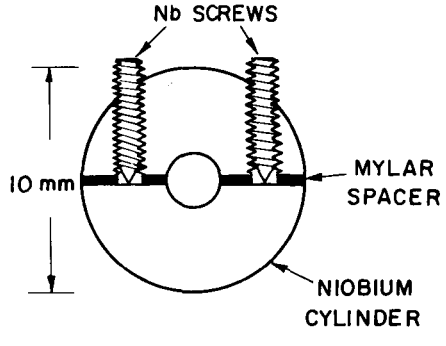

Fig. 8. Point contact dc SQUID

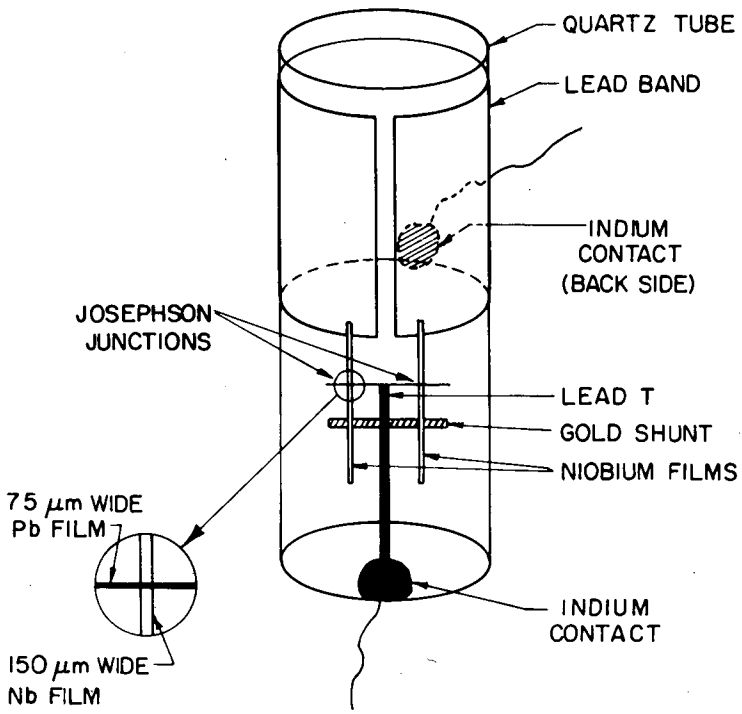

Fig. 9. Thin-film tunnel-junction dc SQUID.

cylinder. (Each niobium film makes a low resistance contact with the gold film, and at low temperatures, a superconducting contact with the Pb/In band.) The niobium is thermally oxidized, and, immediately afterwards, a 3000 Å thick Pb/In tee is deposited. The crossbar of the T overlaps the niobium strips to form two tunnel junctions, each with an area of about 10^{-2} mm^2. The stem of the tee bisects the gold strip between the niobium films to form a shunt for each junctions. Next, the Pb/In band is scribed with a razor blade midway between the niobium strips. Two indium beads are pressed on as contacts, one on the base of the tee, and the other on the Pb/In band on the reverse side of the cylinder. The entire sensor is coated with a thin insulating layer of Duco cement, applied by immersing the sensor in a solution of 1 part Duco cement in 5 parts (by volume) acetone. Finally, a 3000 Å thick Pb/In ground plane (not shown in Fig. 9) is evaporated over the front surface of the SQUID. The ground plane reduces flux leakage through the slit in the Pb/In band and minimizes the inductance of the various metal strips. A 500 Å overlay of silver is deposited on top of the ground plane to protect the Pb/In film from oxidation.

Typical parameters for the sensor are: Capacitance per junction — 200 pF; total critical current per junction — 1 to 5 μA; and parallel shunt resistance — 0.5Ω. The free standing inductance of the cylindrical part of the SQUID is approximately 0.75 nH, while the (parasitic) inductance of the niobium and Pb/In strips is estimated to be about 0.5 nH.

For most applications, it is essential to screen the SQUID from environmental magnetic field fluctuations. Excellent shielding may be obtained by mounting the SQUID inside a cylindrical tube machined from lead, 50/50 tin-lead solder, or niobium, as shown in Fig. 10. The SQUID is mounted on two Delrin rods inserted in support screws, as shown. The ac modulation and feedback coil (see Section III-C), typically two turns of 50 μm diameter Formvar-covered niobium wire of inductance 10 nH, is wound on one of these rods. It is essential that the whole structure be very rigidly mounted to avoid microphonic noise. The cylinder also acts as a ground plane to reduce the inductance of the SQUID cylinder to roughly 0.5 nH. Thus the total SQUID inductance is about 1 nH.

It is usually necessary to couple external signals into the SQUID by means of a superconducting coil coupled as closely as possible to the SQUID. We have made satisfactory coils in the following way. The coil is wound from 75 μm diameter insulated niobium wire on a teflon rod whose diameter is about 50 μm greater than the outer diameter of the SQUID. The coil is coated with Duco cement, and, when the cement is dry, the coil is carefully removed from the teflon rod and mounted on the SQUID. A typical 24-turn single-layer coil had the following parameters: L_i = 356 nH, M_i = 11.5 nH, and $\alpha \approx 0.6$.

To operate the SQUID, the bias current, I_0, is varied (with the feedback loop open) until a maximum value of V_T is obtained. Typically, $I_0 \approx 1.3\ I_m$. At this bias point, r_D is about 1Ω, and the tank circuit Q

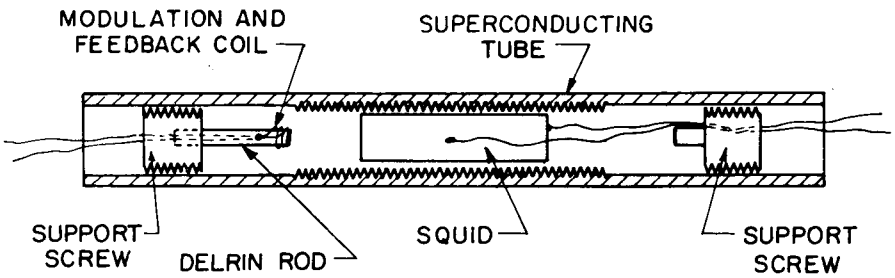

Fig. 10. SQUID mounted in superconducting shield.

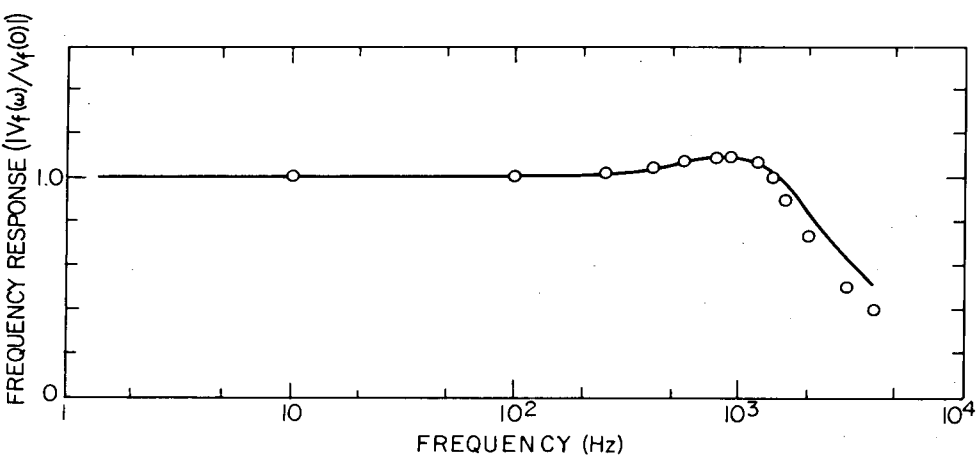

Fig. 11. Typical frequency response for flux-locked dc SQUID: solid line is theoretical, and circles are measured data.

is about 150. The impedance $Q^2 r_D$ presented to the FET is, therefore, about 20 kΩ, somewhat below the value for optimum noise performance. The dynamic range of the flux-locked SQUID in a 1 Hz bandwidth is about $\pm 3 \times 10^6$. A typical frequency response (open circles) for the system is shown in Fig. 11, compared with the theoretical curve (solid line). The response is approximately flat from 0 to 1 kHz.* A typical slewing rate is $2 \times 10^4 \Phi_o \text{sec}^{-1}$*. A detailed discussion of the frequency response and slewing rate has been given elsewhere [14].

A typical noise power spectrum for the dc SQUID in a superconducting shield is shown in Fig. 12. The left-hand ordinate is labeled in units of S_Φ, and the right-hand ordinate is labeled in units of $S_\Phi / 2\alpha^2 L$ for the 24-turn coil described previously. The power spectrum was taken by digitizing the signal from the output of the flux-locked system, and storing the digitized signal in a PDP-11/20 computer. A fast Fourier transform of this signal was taken, squared, and stored, and the process repeated, typically 30 times, to obtain an averaged power spectrum.

The noise of the SQUID is nearly white between 2×10^{-2} Hz and 200 Hz, with a rms value of about $3.5 \times 10^{-5} \Phi_o \text{Hz}^{-1/2}$. The energy resolution for the 24-turn coil is about $7 \times 10^{-30} \text{JHz}^{-1}$. The roll-off above 200 Hz is a result of filtering in the electronics. The rms noise predicted by Eq. (31) with $(\partial V_T / \partial \Phi_e)_{I_o} = 150\ \mu\text{V}/\Phi_o$ (measured), $I_o/I_m = 1.3$, $L = 10^{-9}$ H, $L_T = 200\ \mu$H, $T = 4.2$ K, $r = 0.5\Omega$, and $S_V^{(p)} = 2 \times 10^{-18} \text{V}^2\text{Hz}^{-1}$ is $3.2 \times 10^{-5} \Phi_o \text{Hz}^{-1/2}$. (The current noise term is negligible because L_T was somewhat below the optimum value.) This calculated value is in remarkably good agreement with the measured value. Given the approximations made in the theory, the excellent agreement must be considered somewhat fortuitous. When the temperature of the SQUID was lowered to 1.8 K, the white noise was reduced to about $2 \times 10^{-5}\ \Phi_o \text{Hz}^{-1/2}$; the excellent agreement is again probably fortuitous. However, the fact that the flux resolution of the SQUID improves as the temperature is lowered demonstrates that the measured noise is dominated by intrinsic thermal noise in the SQUID.

Below 2×10^{-2} Hz, the power spectrum varies approximately as 1/f, with a mean square value of about $10^{-10}\ (1\ \text{Hz}/f)\ \Phi_o^2\ \text{Hz}^{-1}$. The origin of this 1/f noise is not firmly established. Clarke and Hawkins [57] measured the 1/f noise in single Josephson junctions, and established that it was generated by equilibrium temperature fluctuations in the junctions. The magnitude of the noise was in good agreement with an appropriately modified version of the theory of Clarke and Voss [58] for 1/f noise in metals. However, the measured 1/f noise power in the SQUID is about two orders of magnitude larger than that expected if the noise originated in thermal fluctuations in the junctions. It is possible that the 1/f noise is produced by the motion of flux pinned in the SQUID or its superconducting shield.

*By replacing the tank circuit with a tuned transformer with a bandwidth of about 20 kHz, we have improved the frequency response to 50 kHz and the slewing rate to $2 \times 10^5\ \Phi_o\ \text{sec}^{-1}$.

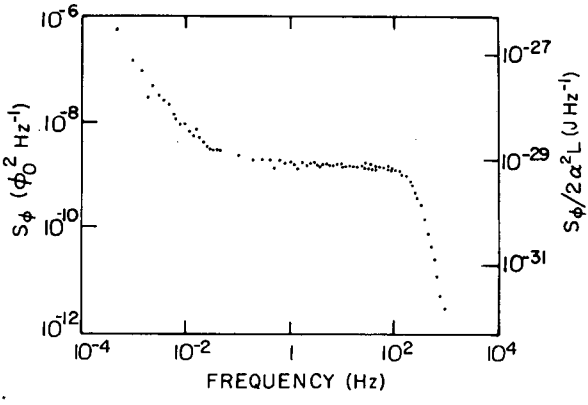

Fig. 12. Typical noise power spectrum for tunnel junction dc SQUID. The right-hand axis specifies the energy resolution with respect to a 24-turn input coil.

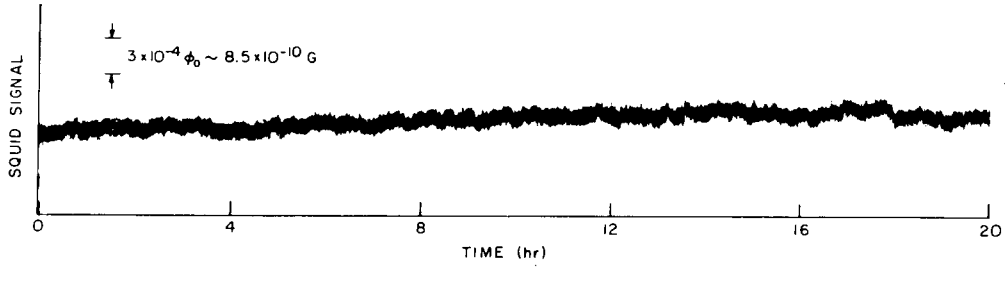

Fig. 13. Long-term drift of a flux-locked SQUID with the temperature of the helium bath regulated at a nominal 4.2 K. The measurement bandwidth is 0 to 0.25 Hz.

The output of the flux-locked SQUID drifted slowly with time. A typical drift observed over a 20 h period is shown in Fig. 13. The average drift is about $2 \times 10^{-5} \Phi_0 h^{-1}$. To achieve this low drift rate, it was necessary to regulate the temperature of the helium both to within ± 50 μK. This regulation was achieved by controlling the pressure of the He^4 vapor in the cryostat. The temperature of the SQUID was measured by a carbon resistor in an ac bridge whose output was used to regulate a valve through which the helium gas was vented. This technique compensated for changes in temperature resulting both from atmospheric pressure fluctuations and from the decrease in hydrostatic pressure of the helium bath as the liquid evaporated.

The drift in the output of the flux-locked SQUID arises from drifts in the temperature of the SQUID. Detailed measurements have been made of this temperature dependence [14]. There are two contributions to the drift. The first contribution is proportional to the change in temperature and to the residual static magnetic field trapped in the superconducting shield around the SQUID. It is likely that the effect arises from the reversible motion of flux lines trapped in the shield as the temperature is changed. The amplitude of the drift produced by a given change in temperature and for a given trapped field depends on the material, being largest for solder, smaller for lead, and smallest for niobium. Niobium is, therefore, the preferred material for the shield. For a niobium shield, the drift was of the order of $1 \Phi_0 K^{-1} G^{-1}$ at 4.2 K.

The second component of temperature-related drift is independent of the trapped magnetic field, and is evident only when the trapped field is small, 10 mG or less [14]. It is thought that this contribution is related to an asymmetry in the SQUID. If the two junctions of the SQUID are not identical, I_0 divides unequally between them, thereby linking flux to the SQUID. If the critical currents change with temperature, the flux generated by I_0 also changes with temperature. The magnitude of the magnetic-field independent component was not greater than $0.1 \Phi_0 K^{-1}$.

Both contributions to the drift can be minimized by regulating the temperature of the helium bath.

E. Future Improvements in the dc SQUID

At frequencies above about 10^{-2} Hz the tunnel-junction dc SQUID is limited by its intrinsic noise. With the present design, no improvements in the noise of the device are possible, except by lowering the temperature. For most applications, it is not practical to operate the SQUID at temperatures other than 4.2 K. From Eq. (31), we see that for the intrinsic noise S_Φ is proportional to L^2/r, and, consequently that $S_\Phi/2\alpha^2 L$ is proportional to L/r.* Thus the figure of merit can be

*It is noteworthy that S_Φ/L is proportional to L/r, the time constant of the SQUID. Under optimum condition, the dc SQUID operates at a Josephson frequency near the frequency r/L; the higher the frequency, the

lowered by decreasing L and/or increasing r. It is not practical to decrease L significantly without also decreasing α: if the cylindrical part of the SQUID is made longer or thinner, the parasitic inductances will become more important. The only way to decrease $S_\Phi/2\alpha^2 L$ is to increase r. Because of the restriction on the hysteresis parameter ($\beta_c = 2\pi I_c R^2 C/\Phi_0 \leq 1$), an increase in r must be accompanied by a reduction in either I_c or r. Because of noise-rounding of the I-V characteristic, it is undesirable to reduce I_c much below its present value, and, therefore, C must be reduced. This reduction can be achieved only by decreasing the area of the tunnel junctions. Since, for fixed β_c, $S_\Phi \propto 1/R \propto C \propto$ area, a reduction in the junction size by four orders of magnitude to 1x1 μm (a size presently attainable by state-of-the-art photoresist techniques) would decrease S_Φ by two orders of magnitude. There is no known reason why such an improvement in resolution should not be obtained in the white noise region. However, it is likely that the reduction in the volume of the junctions would increase the 1/f noise. In the present SQUID, the measured 1/f noise power spectrum is two orders of magnitude greater than that expected from the intrinsic 1/f noise in the junctions, which is inversely proportional to the junction volume. Thus a four-order-of-magnitude reduction in the junction volume is expected to increase the 1/f noise power spectrum of the SQUID by two orders of magnitude.

IV. RF SQUID

A. Theory of the rf SQUID

The operation of the rf SQUID has been described by a number of authors [7-9, 15, 40, 59]. I shall generally follow the description given in my earlier article [15], but include recent ideas of Jackel and Buhrman [40] that are important in the subsequent noise analysis.

The rf SQUID (Fig. 14) consists of a superconducting ring of inductance L (typically 10^{-9} H) containing a single Josephson junction of critical current I_c, shunted by a resistance R and a capacitance C. We assume that the junction obeys the sinusoidal current-phase relation [Eq. (4)], and that $\beta_c \ll 1$, so that the I-V characteristic is non-hysteretic (the cases with a non-sinusoidal current-phase relation and hysteretic I-V characteristics are described by Jackel and Buhrman [40]). The critical current is usually chosen to be about Φ_0/L.

Fluxoid quantization [60] imposes the constraint

$$\theta + 2\pi\Phi/\Phi_0 = 0 \qquad (34)$$

---

better is the energy resolution. The upper limit on the Josephson frequency is Δ/h, about 3×10^{11} Hz in lead or niobium, although quasiparticle relaxation processes may set an appreciably lower limit.

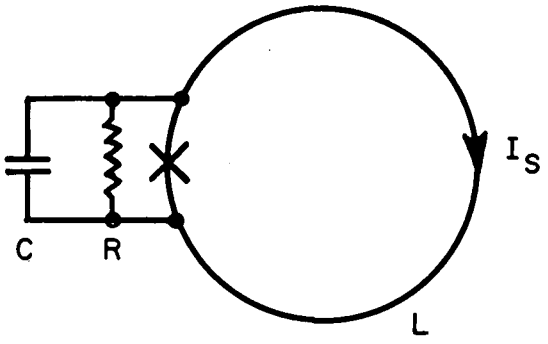

Fig. 14. Configuration of rf SQUID.

on the flux Φ threading the ring and the phase difference θ across the junction. The phase difference θ determines the current I_s flowing around the ring,

$$I_s = -I_c \sin(2\pi\Phi/\Phi_o) \quad . \tag{35}$$

A quasistatic external flux Φ_e will thus give rise to a total flux

$$\Phi = \Phi_e - LI_c \sin(2\pi\Phi/\Phi_o) \tag{36}$$

in the ring. The variation of Φ with Φ_e is sketched in Fig. 15(a) for $LI_c = 1.25\Phi_o$. The regions with positive slope are stable, whereas those with negative slope are not. Suppose that Φ_e is now slowly increased from zero (Fig. 15(b)). The total flux Φ will increase less rapidly than Φ_e as the circulating current I_s tends to screen out Φ_e; if the ring were completely superconducting, the screening would be exact, and Φ would remain at zero. When I_s just exceeds I_c, at an applied flux Φ_{ec} and an enclosed flux Φ_c, the junction switches momentarily into a non-zero voltage state, and the SQUID jumps from the $k = 0$ quantum state into the $k = 1$ quantum state. The time for this transition is $\sim L/R$. If Φ_e is increased further, the SQUID will make transitions into the $k = 2, 3 \ldots$ states at $\Phi_e = \Phi_c + \Phi_o, \Phi_c + 2\Phi_o, \ldots$. Suppose Φ_e is now decreased from just above Φ_c . The SQUID will remain in the $k = 1$ state until $\Phi_e = \Phi_o - \Phi_c$, at which point I_s again exceeds the critical current and the SQUID returns to the $k = 0$ state. In the same way,

as Φ_e is lowered to below $-\Phi_c$ and then increased again, a second hysteresis loop will be traced out.

This hysteretic behavior occurs if $LI_c > \Phi_o/2\pi$ for a sinusoidal current-phase relation. If $LI_c < \Phi_o/2\pi$, no hysteresis occurs: SQUIDs operated in this limit are in the so-called "inductive mode" [31,61]. In this article we shall be concerned only with the "hysteretic mode" in which most SQUIDs are operated. We also note that in practice, thermodynamic fluctuations cause transitions between quantum states to occur at lower values of Φ_e than those just described. The resultant uncertainty in the value of Φ_e at which transitions occur is the source of intrinsic noise (see Section IV-D).

The energy ΔE dissipated in going around a single hysteresis loop is given by the area of the loop divided by L. By inspection of Fig. 5(b), we find

$$\Delta E = \Phi_o (2\Phi_{ec} - \Phi_o)(1 - \Phi_c/\Phi_{ec})/L \sim \Phi_o I_c \qquad (37)$$

if $LI_c \sim \Phi_o$ and $\Phi_c/\Phi_{ec} << 1$.

We now consider the rf operation of the SQUID. The SQUID is inductively coupled to the coil of an LC-resonant circuit, as shown in Fig. 16. L_T, C_T, and R_T are the inductance, capacitance, and parallel resistance of the tank circuit, and $\omega/2\pi$ is the resonant frequency, typically a few tens of MHz. The tank circuit is excited at its resonant frequency by an rf current $I_{rf}\sin\omega t$, and the voltage across the tank circuit is amplified by a preamplifier with a high input impedance. Suppose initially that $\Phi_e = 0$. When I_{rf} is very small, the peak flux applied to the ring, $MI_T = QMI_{rf}$, is less than Φ_{ec}, and no dissipation occurs in the SQUID ($Q = R_T/\omega L_T$, $M^2 = K^2 LL_T$, and I_T is the peak current in the tank coil). The tank circuit voltage, V_T, is initially a linear function of I_{rf}, as shown in Fig. 17. As I_{rf} is increased, the peak flux will equal Φ_{ec} when $I_T = \Phi_{ec}/M$ or $I_{rf} = \Phi_{ec}/MQ$, at A in Fig. 17. The corresponding peak voltage across the tank circuit is

$$V_T^{(n)} = \omega L_T \Phi_{ec}/M \quad , \qquad (38)$$

where the suffix (n) indicates $\Phi_e = n\Phi_o$, in this case with $n = 0$. At this point, the SQUID makes a transition to either the $k = +1$ or the $k = -1$ state, depending on the direction of the rf flux. Later in the rf cycle, the SQUID returns to the $k = 0$ state. As the SQUID traverses the hysteresis loop, energy ΔE is extracted from the tank circuit. Because of this loss, the peak flux on the next half-cycle does not exceed the critical flux, and no transition occurs. The tank circuit takes many cycles to recover sufficient energy to induce a further transition; this transition may be into either the $k = +1$ or $k = -1$ states. In practice, the

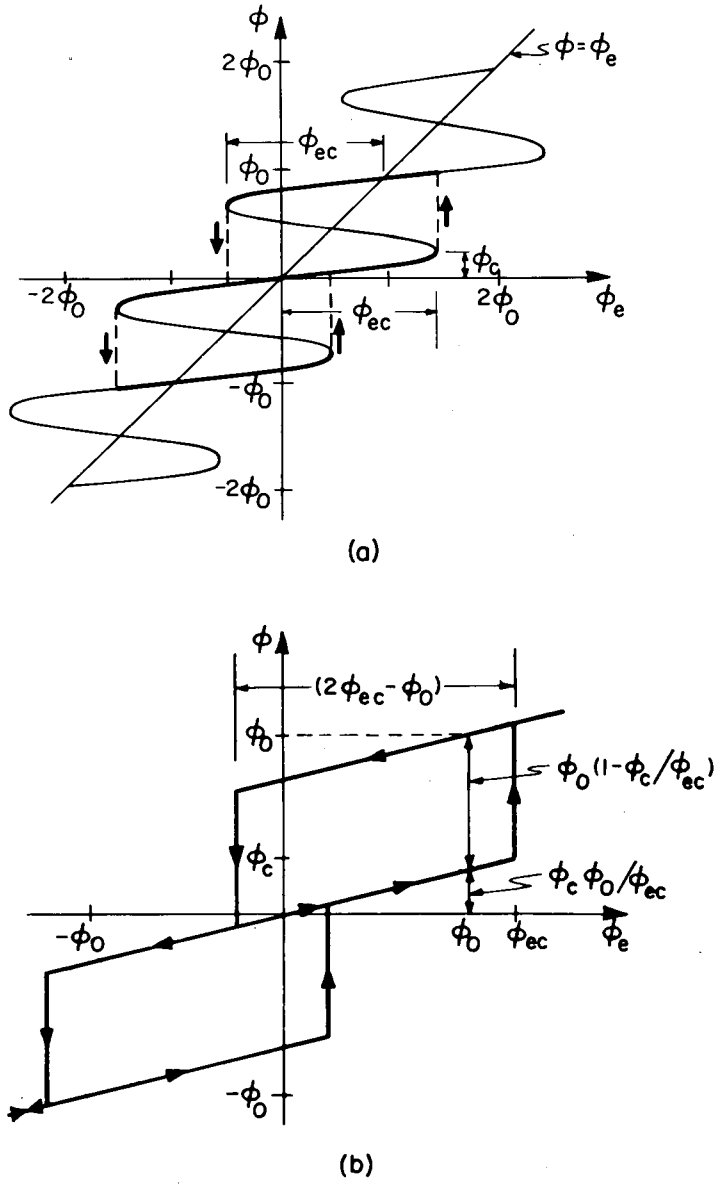

Fig. 15. rf SQUID: (a) plot of enclosed flux (Φ) vs Φ_e for $LI_c = 1.25\ \Phi_0$; (b) values of Φ as Φ_e is slowly increased and then decreased.

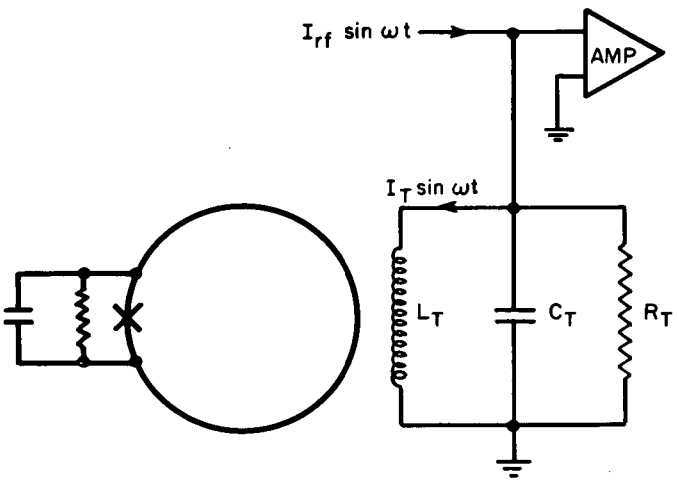

Fig. 16. Tank circuit inductively coupled to rf SQUID.

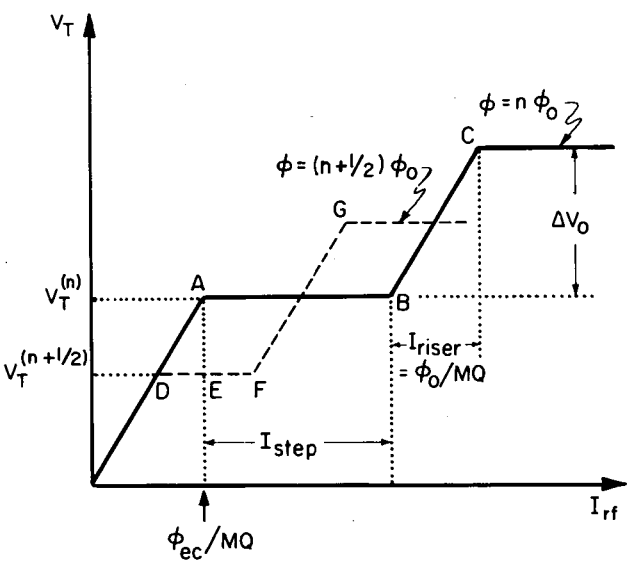

Fig. 17. V_T vs I_{rf} for rf SQUID in absence of thermal fluctuations.

slow recovery of V_T after each pair of transitions is not observed, probably because the fraction loss of tank circuit energy [$\Delta E/(L_T\Phi_{ec}^2/2M^2) \sim 2K^2$ if $LI_c \sim \Phi_o$] is rather small, and the V_T vs I_{rf} curves are appreciably noise-rounded in practice.

If I_{rf} is now increased, transitions occur at the same values of I_T and V_T, but because energy is supplied at a higher rate, the stored energy builds up more rapidly after each transition, and transitions occur more frequently. As I_{rf} is increased, the "step" AB in Fig. 17 is traced out. At the midpoint of AB, a transition occurs once each cycle on either the positive or negative peak of the rf cycle. At B, a transition is induced on each positive and negative peak. The excess power supplied at B over that at A is just $2\Delta E(\omega/2\pi)$, the power dissipated when two hysteresis loops are traversed on each rf cycle.

The length of the step AB is given by [40]*

$$V_T^{(n)} I_{step}/2 = 2\Delta E(\omega/2\pi) \tag{39}$$

or

$$I_{step} \approx 2I_c M/\pi L_T , \tag{40}$$

where we have used Eqs. (37) and (38), and assumed $\Phi_{ec} \approx \Phi_o$.

A further increase in I_{rf} beyond B produces a "riser" BC (see Fig. 17). At C, transitions from the $k = \pm 1$ to the $k = \pm 2$ states occur. The rf flux applied to the SQUID is Φ_{ec} at B and $(\Phi_{ec} + \Phi_o)$ at C. Thus $I_{riser} = \Phi_o/MQ$. In an analogous way, a series of steps and risers is observed as I_{rf} is further increased. The separation of successive steps is

$$\Delta V_o = Q I_{riser} \omega L_T = \omega L_T \Phi_o/M \quad . \tag{41}$$

Now apply a positive external flux $\Phi_e = \Phi_o/2$ to the SQUID. This flux has the effect of shifting the hysteresis loops of Fig. 14 by $\Phi_o/2$. Thus a transition will occur on the positive peak of the rf cycle at a flux equal to $(\Phi_{ec} - \Phi_o/2)$, whereas on the negative peak, the required flux is $(\Phi_{ec} + \Phi_o/2$. Thus as I_{rf} is increased from zero, the first step will occur at D in Fig. 17 when

---

*Note that $V_t^{(n)}$ and I_{step} are peak rather than rms values, so that the power dissipation is $V_T^{(n)} I_{step}/2$, assuming that the voltage and current are in phase.

$$V_T^{(n+1/2)} = \omega L_T (\Phi_{ec} - \Phi_o/2)/M \ . \qquad (42)$$

As I_{rf} is increased along DF, only one hysteresis loop is traversed, corresponding to the k = 0 to k = 1 transition at $(\Phi_{ec} - \Phi_o/2)$. As I_{rf} is further increased, V_T rises to G, with I_{riser} again equal to Φ_o/MQ. At G, transitions at a peak rf flux - $(\Phi_{ec} + \Phi_o/2)$ begin. Thus a series of steps and risers is obtained for $\Phi_e = \Phi_o/2$, interlocking those obtained for $\Phi_e = 0$.

As Φ_e is increased from 0 to $\Phi_o/2$, the value of V_T at which the first step occurs steadily decreases. For $0 < \Phi_e < \Phi_o/2$ the first step splits into two distinct steps, the lower corresponding to the transition between k = 0 and k = 1 at an rf flux $(\Phi_{ec} - \Phi_e)$, and the upper corresponding to the transition between k = 0 and k = -1 at an rf flux $(\Phi_{ec} + \Phi_e)$. For the special case $\Phi_e = \Phi_o/2$, the steps corresponding to the transitions between k = 0 and k = -1 and those between k = 1 and k = 2 occur at the same value of V_T. The steps for higher order transitions are similarly split except when $\Phi_e = 0$ or $\Phi_o/2$. For $\Phi_o/2 < \Phi_e \leq 3\Phi_o/2$, the lowest energy state of the SQUID in the absence of rf flux is the k = 1 state. Thus, in this range, the lowest order transitions induced by the rf flux are from the k = 1 to the k = 0 and 2 states. As Φ_e is increased from $\Phi_o/2$ to Φ_o, V_T increases from $V_T^{(n+1/2)}$ to $V_T^{(n)}$. In an analogous way, as Φ_e is steadily increased, the voltage at which the first step occurs oscillates between $V_T^{(n)}$ and $V_T^{(n+1/2)}$ with period Φ_o. The modulation amplitude $\Delta V_T^{(\Phi_o/2)} = V_T^{(n)} - V_T^{(n+1/2)}$ is given by subtracting Eq. (42) from Eq. (38):

$$\Delta V_T^{(\Phi_o/2)} = \omega L_T \Phi_o/2M \ . \qquad (43)$$

The incremental change in V_T for a small change $\delta\Phi_e$ $(\Phi_e \neq n\Phi_o/2)$ is

$$\delta V_T = \omega L_T \delta\Phi_e/M \ . \qquad (44)$$

For given values of L_T and L, Eqs. (43) and (44) imply that the sensitivity can be made arbitrarily high by making the coupling coefficient K arbitrarily small. However, K obviously cannot be made so small that the SQUID has a negligible influence on the tank circuit, and we need to find a lower limit on K. In order to operate the SQUID, one must be able to choose a value of I_{rf} that lies on the first step for all values of Φ_e. This requirement, namely that F (in Fig. 17) lie to the right of A, or that DF must exceed DE, sets a lower bound on K. The power dissipation in the SQUID is zero at D and $\Delta E(\omega/2\pi)$ at F. Hence, $\left(I_{rf}^{(F)} - I_{rf}^{(D)}\right) V_T^{(n+1/2)}/2 = \Delta E(\omega/2\pi)$ (I_{rf} and V_T are peak

values rather than rms values). If we note that $I_{rf}^{(E)} - I_{rf}^{(D)} = \Phi_o/2MQ$, and use Eqs. (37) and (42), the criterion DF ≥ DE becomes (with $\Phi_{ec} = \Phi_o$)

$$K^2 Q \geq \pi/4 \tag{45}$$

This result is only approximate because we have assumed in this discussion that the SQUID dissipation is much larger than the dissipation in R_T.

B. Operation of the rf SQUID

A typical (simplified) circuit for the operation of the rf SQUID is shown in Fig. 18. The rf oscillator is adjusted so that the SQUID is biased on the first step of the V_T vs I_{rf} curve for all values of Φ_e. The rf voltage across the tank circuit is amplified with a low-noise preamplifier (usually with an FET input stage) that has a high input impedance. After further amplification the rf signal is demodulated (sometimes with a diode as shown in Fig. 18, although often a more sophisticated demodulation scheme is used), and the demodulated signal is integrated. The smoothed output is periodic in Φ_e. An ac modulation flux, at a frequency of typically 100 kHz, and with a peak-to-peak amplitude $\leq \Phi_o/2$, is also applied to the SQUID, just as in the case of the dc SQUID. The signal at the output of the rf integrator, therefore, contains both 100 kHz and 200 kHz components, depending on the value of Φ_e. This signal is lock-in detected at the modulation frequency, integrated, amplified, and fed back as a current in the modulation coil. The rf SQUID is thus operated in a feedback mode in the same manner as the dc SQUID.

C. Noise in the rf SQUID

There are three sources of white noise that we should consider: intrinsic noise, tank circuit noise, and preamplifier noise. A discussion of low frequency noise will be deferred until Section IV-C.

In the previous section, we assumed that all transitions occurred when $\Phi_e = \Phi_{ec}$; in practice, this is not the case. The SQUID has a nonzero probability of making a transition at $\Phi_e < \Phi_{ec}$. Each time Φ_e is increased from zero, the k = 0 to k = 1 transition occurs at a different value of Φ_e. For a sinusoidal current-phase relation and when $d\Phi_e/dt = \text{const} \ll \Phi_o R/L$, Kurkijärvi [62] showed that the distribution in values of Φ_e at which the transitions occur was

$$\sigma = (3\pi/2\sqrt{2})^{2/3} \sigma_o L I_c (k_B T/\Phi_o I_c)^{2/3} , \tag{46}$$

where T is the SQUID temperature, and $\sigma_o \approx 1$. For T = 4 K, L = 10^{-9} H, and $LI_c = \Phi_o$, $\sigma \approx 0.13\ \Phi_o$. Equation (46) has been experimentally verified [63, 64].

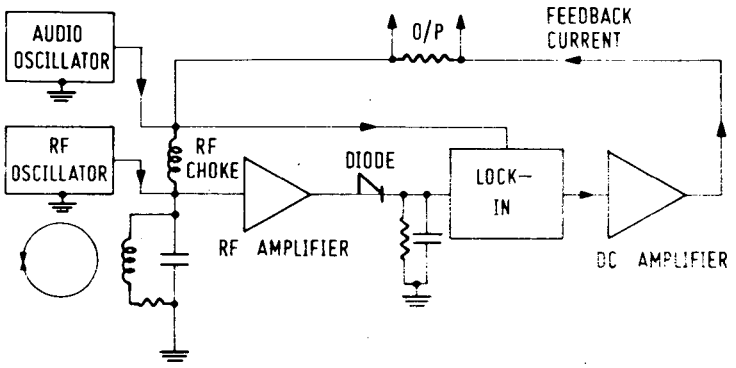

Fig. 18. Simplified schematic of rf SQUID in flux-locked loop.

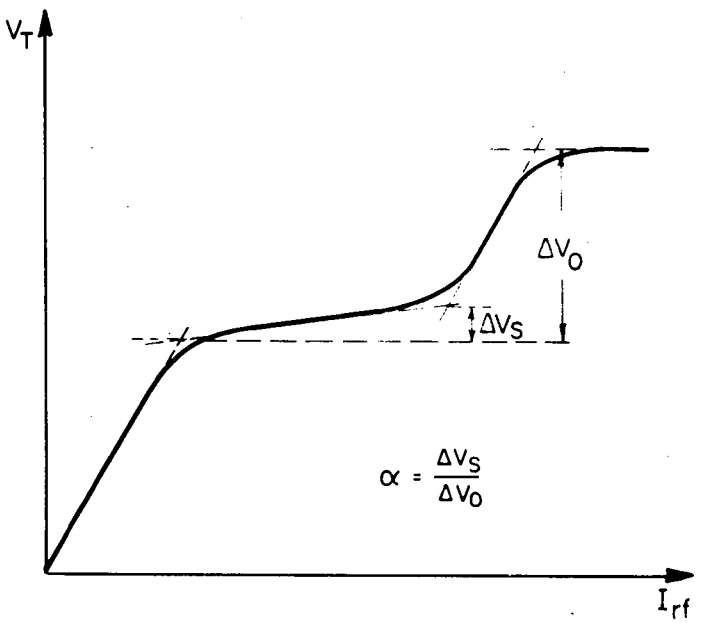

Fig. 19. V_T vs I_{rf} for rf SQUID in presence of thermal fluctuations.

When the SQUID is driven with an rf flux, the fluctuations in the value of flux at which transitions occur have two consequences. First, Kurkijärvi and Webb [65] showed that V_T will fluctuate, giving an equivalent intrinsic flux noise power spectrum

$$S_\Phi^{(i)} \approx 0.7(3\pi/2\sqrt{2})^{4/3}(2\pi/\omega)\, L^2 I_c^{2/3} (k_B T/\Phi_o)^{4/3} \quad . \tag{47}$$

If the current-phase relation is non-sinusoidal, the noise will be higher than that predicted by Eq. (47) [40,66]. Second, the noise will round the step edges and cause the steps to tilt [65], so that the voltage increases from A to B (see Fig. 19). This tilting arises in the following way [66]. In the absence of thermal fluctuations, the transition from the $k = 0$ to the $k = 1$ state occurs at a precisely defined value of flux ($\Phi_e + \Phi_{rf}$). However, in the presence of thermal fluctuations, the transition has a certain probability of occurring at a lower value of flux. Just to the right of A (Fig. 17), a transition occurs at the peak of the rf flux only once in many rf cycles. The SQUID, therefore, makes many attempts at any given transition, and the probability of its occurring in any one cycle is small. Just to the left of B, a transition must occur at each peak value of the rf flux, with unity probability. To increase the probability of the transition, the peak value of the rf flux increases slightly, so that V_T also increases as I_{rf} is increased from A to B. Following Jackel and Buhrman [40], we introduce a parameter α, the ratio of the voltage rise along a step, ΔV_s, to the separation in voltage of successive steps, ΔV_o (see Fig. 18). Jackel and Buhrman [40] show that α is related to $S_\Phi^{(f)}$ by the relation

$$\alpha^2/(1-\alpha)^2 \approx S_\Phi^{(i)} \omega/\pi \Phi_o^2 \quad . \tag{48}$$

They have verified this relation experimentally, and shown that, apart from small changes in the numerical factor, it remains valid even when the current-phase relationship is non-sinusoidal [40].

The fact that the step is tilted modifies Eq. (44) to

$$\delta V_T' = (1 - \alpha)\omega L_T \delta\Phi_e/M \quad . \tag{49}$$

We consider next the tank circuit noise. The tank circuit resistance R_T produces a Johnson noise current in the inductance L_T that adds to I_{rf} [60]. At a given value of I_{rf}, these currents cause the bias point of the SQUID to fluctuate. Because the steps are tilted (dV_T/dI_{rf} is non-zero), the Johnson noise contributes to the SQUID noise. Following Jackel and Buhrman [40], we calculate the equivalent flux noise of this contribution. From Fig. 19, and Eqs. (40) and (41)*, assuming $< I_c \approx \Phi_o$, we find

*See footnote to Eqs. (39) and (40).

$$\left.\frac{dV_T}{dI_{rf}}\right|_{step} = \frac{\alpha \Delta V_o}{I_{step}} \approx \frac{\pi \alpha \omega L_T}{2K^2} \quad . \tag{50}$$

We define the effective Q on a step as

$$Q_{eff} = \left.\frac{dV_T}{dI_{rf}}\right|_{step} \Big/ \omega L_T \approx \frac{\pi \alpha}{2K^2} \quad , \tag{51}$$

where we have used Eq. (50).

The spectral density of the current noise in the inductance L_T at the resonant frequency of the tank circuit is

$$S_I^{(tc)} = \frac{4k_B T_e}{R_T} = \frac{4k_B T_e}{Q \omega L_T} \quad , \tag{52}$$

where $Q = R_T/\omega L_T$ is the quality factor of the parallel resonant circuit. T_e is the effective temperature of the tank circuit; with a room temperature amplifier, T_e might be 200 K [40]. The corresponding voltage spectral density (from the first equality of Eq. (51)) is

$$S_V^{(tc)} = Q_{eff}^2 \omega^2 L_T^2 S_I^{(tc)} \quad . \tag{53}$$

The equivalent flux noise due to the tank circuit is, using Eqs. (49), (51), and (53), and setting $K^2 Q = \pi/4$,

$$S_\Phi^{(tc)} = \frac{M^2 S_v^{(tc)}}{(1-\alpha)^2 \omega^2 L_T^2} \approx \frac{4\pi\alpha^2}{(1-\alpha)^2} \frac{k_B T_e L}{\omega} \quad . \tag{54}$$

The preamplifier also contributes to the total SQUID noise. The spectral density of the preamplifier voltage noise, $S_V^{(p)}$, is equivalent to a flux noise spectral density (from Eq. (49))

$$S_\Phi^{(p)} = \left[\frac{M}{\omega L_T (1-\alpha)}\right]^2 S_v^{(p)} \quad . \tag{55}$$

We define a noise temperature, $T_N^{(p)}$, for the preamplifier through the relation

$$S_V^{(p)} = 4k_B T_N^{(p)} \left(\partial V_T/\partial I_{rf}\right)_{step} \approx 2\pi\alpha\omega L_T k_B T_N^{(p)}/K^2 \quad . \tag{56}$$

If we take as typical values $[S_V^{(p)}]^{1/2} \approx 2\text{nVHz}^{-1/2}$, $\alpha \approx 0.2$, $\omega/2\pi \approx 30$ MHz, $L_T \approx 5\times10^{-7}$ H, and $K^2 \approx 0.2$, we find $T_N \approx 50$ K. From Eqs. (55) and (56) we obtain

$$S_\Phi^{(p)} \approx \frac{2\pi\alpha}{(1-\alpha)^2} \frac{k_B T_N^{(p)} L}{\omega} \quad . \tag{57}$$

The energy resolution is found from Eqs. (48), (54), and (57):

$$\frac{S_\Phi}{2L} \approx \frac{\alpha}{(1-\alpha)^2} \left\{ \underbrace{\frac{\pi\alpha\Phi_o^2}{2\omega L}}_{\text{intrinsic}} + \underbrace{\frac{2\pi\alpha k_B T_e}{\omega}}_{\substack{\text{tank}\\ \text{circuit}}} + \underbrace{\frac{\pi k_B T_N^{(p)}}{\omega}}_{\text{preamplifier}} \right\} \quad . \tag{58}$$

Note that Eq. (58) assumes that $LI_c \approx \Phi_o$. The intrinsic energy resolution is proportional to the energy available per cycle, $\sim \Phi_o^2/L$, divided by the sampling frequency, ω. The second and third terms represent the thermal energies of the tank circuit ($k_B T_e$) and preamplifier ($k_B T_N^{(p)}$) divided by ω. It should be emphasized that these expressions are approximate, and that more detailed estimates of the noise may differ by factors of 2 or 3 [40].

It is instructive to make estimates for the three contributions. If we take as typical values $\alpha \approx 0.2$, $L \approx 10^{-9}$ H, $\omega/2\pi \approx 30$ MHz, $T_e \approx 200$ K, and $T_N^{(p)} \approx 50$ K, we find $S_\Phi^{(i)}/2L \approx 2\times10^{-30}\,\text{JHz}^{-1}$, $S_\Phi^{(tc)}/2L \approx 6\times10^{-30}\,\text{JHz}^{-1}$, $S_\Phi^{(p)}/2L \approx 4\times10^{-30}\,\text{JHz}^{-1}$, and $S_\Phi/2L \approx 12\times10^{-30}\,\text{JHz}^{-1}$. The combined rms flux noise is $S_\Phi^{1/2} \approx 8\times10^{-5}\,\Phi_o\text{Hz}^{-1/2}$. In this example, the tank circuit noise is slightly greater than the preamplifier noise. From Eqs. (55) or (56) we see that $S_\Phi^{(p)} \propto K^2$, whereas Eqs. (51), (53), and the first equality of Eq. (54) yield $S_\Phi^{(tc)} \propto 1/K^2$, for constant Q. Thus the overall resolution could be (very slightly) improved by increasing K so that $S_\Phi^{(p)} = S_\Phi^{(tc)}$ and $K^2Q > \pi/4$. The intrinsic noise is relatively insignificant, as is usually the case for SQUIDs operated at 30 MHz. Jackel and Buhrman [40] have given a detailed discussion of the optimization of the flux resolution.

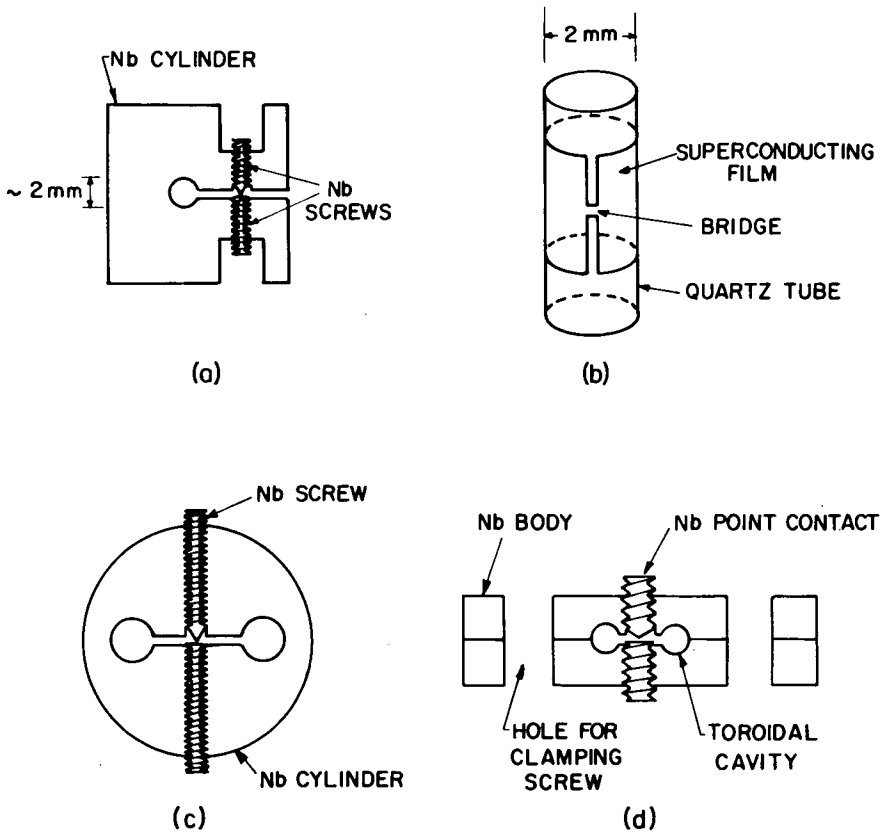

Fig. 20. Selection of rf SQUIDS: (a) point-contact rf SQUID, machined from niobium; (b) thin-film rf SQUID evaporated on quartz tube; (c) two-hole point-contact rf SQUID, machined from niobium; (d) toroidal point-contact rf SQUID, machined from niobium.

D. Practical rf SQUIDs: Fabrication and Performance

A variety of rf SQUID configurations have been used. The earliest versions are shown in Figs. 20(a) and 20(b). The point contact SQUID of Zimmerman et al. [7], Fig. 20(a), was manufactured from a solid cylinder of niobium. The point contact was usually adjusted while it was at liquid helium temperatures to obtain the optimum critical current. A more robust version incorporating a glass spacer in the slot was developed by Buhrman et al. [38]; this SQUID could be recycled without resetting the point contact. The tank circuit coil was rigidly mounted inside the cylinder. Mercereau and co-workers [8] used the thin film rf SQUID shown in Fig. 20(b). A thin film of superconductor (usually a tin alloy or niobium) was evaporated around a quartz or sapphire tube typically 2 mm in diameter and 20 mm long. A single Anderson-Dayem bridge [30] or Notarys bridge [31] was then formed in the superconducting cylinder. Similar devices have been used by Goodman et al. [67] and Opfer et al. [68], and are commercially available from S.C.T. [12] and Develco [10]. The tank coil is placed inside the SQUID or wound around it. A further development of the point contact device is the symmetric rf SQUID [7, 9, 13, 69] shown in Fig. 20(c). Two holes drilled through a niobium cylinder are connected by a slot across which there is an adjustable niobium point contact. The inductance of this SQUID is approximately one-half that of a single-loop SQUID with the same total area. The two-hole SQUID can be recycled successfully without readjusting the niobium screw. A thin-film two-hole SQUID using tunnel junctions has been operated by Ehnholm et al. [70].

A particularly useful point contact configuration is the toroidal SQUID [67, 71] shown in Fig. 20(d). The SQUID is made in two halves that form a toroidal cavity when clamped together. The toroid is connected on its inner surface by a disk-shaped cavity containing a point contact. The tank circuit coil and input coil are placed inside the toroidal cavity. The toroidal SQUID has several advantages: it is extremely rugged; it is self-shielding against external magnetic field fluctuations; its inductance can be rather low, as the length of the cavity is relatively long; and large inductance signal coils can be used. Toroidal rf SQUIDs are commercially available from both S.C.T. [12] and S.H.E. [13].

Yet another very ingenious point contact device, the fractional turn SQUID, has been operated by Zimmerman [72, 73]. This SQUID contains twelve loops in parallel connected across a single point contact. The effective inductance of the SQUID is thereby reduced, since the loop inductances are in parallel, so that the signal available from the SQUID is enhanced. Ehnholm et al. [70] have fabricated a thin-film SQUID with eight loops in parallel across a Nb-NbO_x-Pb tunnel junction.

These devices are most commonly operated at a frequency of about 30 MHz. The inductance, L, of the devices shown in Figs. 20(a)-(c) is 10^{-9} H or less, and their critical current, I_c, is about $\Phi_o/L \sim 2\mu$A. In the feedback mode, a dynamic range of 10^6 to 10^7 in a 1 Hz bandwidth, a frequency response that is essentially flat from 0 to several kHz, and a slewing

rate of 10^4 to 10^6 $\Phi_0\,s^{-1}$ are typical. The flux noise of these devices is usually stated to be white, with an rms value of about $10^{-4}\,\Phi_0 Hz^{-1/2}$. This value is in good agreement with the value estimated in Section IV-C.

In the summer of 1975 we measured the noise power spectra for the toroidal SQUIDs available from S.C.T. and S.H.E. using the facilities available at Berkeley [74]. The power spectra obtained, plotted as $S_\Phi/2\alpha^2L$, are shown in Fig. 21, together with the power spectrum for the dc SQUID. The S.H.E. SQUID had a resistor connected to the input coil that contributed about one-third of the mean square white noise. Since these spectra were taken, the white noise of the S.H.E. SQUID has been reduced to about 5×10^{-29} JHz^{-1} : this value is indicated on the graph. All three SQUIDs exhibit 1/f noise at low frequencies. The value of S_Φ, M_i, L_i and $S_\Phi/2\alpha^2L$ (in the white noise region) are presented in Table I for five SQUIDs (in the case of the S.H.E. SQUID, the new value of S_Φ has been used).

There have been several attempts to obtain lower noise by working at higher frequencies. The high frequency work was initially motivated by the observation that the signal available from the rf SQUID is proportional to ω, as indicated in Eq. (43). Thus Zimmerman and Frederick [75] and Kamper and Simmonds [76] operated SQUIDs at 300 MHz and 9 GHz respectively, and observed an increase in the available signal that was close to that predicted. They did not report measurements of the noise. It should be realized that an increase in operating frequency does not automatically improve the noise performance since the noise of preamplifiers also tends to increase with frequency. For example, Clark and Jackel [77] operated a SQUID at 450 MHz, and although their rms flux noise was somewhat lower than that of most 30 MHz SQUIDs, the figure of merit $S_\Phi/2\alpha^2L$ was about 5×10^{-29} JHz^{-1}, comparable with the best 30 MHz SQUIDs (see Table I). However, Pierce et al. [78] operated a thin film cyclindrical SQUID at 10 GHz, and obtained a rms flux noise of about $10^{-5}\,\Phi_0 Hz^{-1/2}$ and $S_\Phi/2\alpha^2L \approx 2 \times 10^{-30}$ JHz^{-1} at frequencies above a few kHz (see Table I). This is the lowest figure of merit I am aware of. Unfortunately, the noise increased appreciably at lower frequencies. The best flux resolution I know of, $7 \times 10^{-6}\,\Phi_0 Hz^{-1/2}$, was achieved by Gaerttner [79] using a 440 MHz SQUID; the parameters required to calculate $S_\Phi/2\alpha^2L$ do not appear to be available.

Table I. Flux noise power spectrum in the white noise region (S_Φ), mutual inductance with input coil (M_i), inductance of input coil (L_i), and figure of merit ($S_\Phi/2\alpha^2 L$) for several SQUIDs.

SQUID	S_Φ (Φ_o^2 Hz^{-1})	M_i (nH)	L_i (nH)	$S_\Phi/2\alpha^2 L$ (10^{-30} JHz^{-1})
dc (Clarke et al. [14])	1.2×10^{-9}	11.5	356	7
rf (S.H.E. [13]) 19 MHz	5×10^{-9}	20	2×10^{3}	50
rf (S.C.T. [12]) 30 MHz	6.6×10^{-10}	3	360	50
rf (Clark and Jackel [77]) 450 MHz	9×10^{-10}	35	3×10^{4}	50
rf (Pierce et al. [78]) 10 GHz	1×10^{-10}	8	500	2

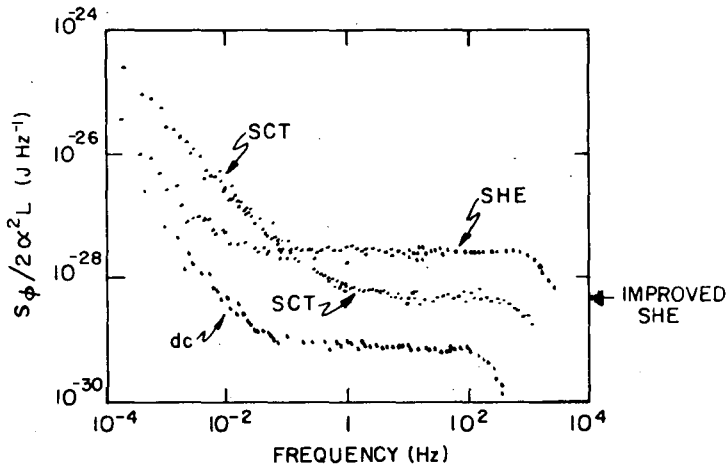

Fig. 21. Noise power spectra (plotted as energy resolution) for tunnel junction dc SQUID and S.C.T. and S.H.E. toroidal rf SQUIDs (Summer 1975). Subsequently, the white noise of the S.H.E. SQUID was improved to the level shown.

E. Future Improvements in the rf SQUID

It appears that SQUIDs operated at about 30 MHz are limited by preamplifier or tank circuit noise rather than by intrinsic noise. The optimization of the performance has been discussed in detail by Jackel and Buhrman [40]. They consider two possible cases: (1) $S_\Phi^{(p)} > S_\Phi^{(tc)}$. From Eqs. (56) and (57) we see that $S_\Phi^{(p)} \propto T_N^{(p)}/\omega \propto 1/Q\omega^2 L_T = 1/\omega R_T$. At a given frequency, one may improve the flux resolution by increasing R_T; (2) $S_\Phi^{(p)} < S_\Phi^{(tc)}$. As noted in Section IV-C, since $S_\Phi^{(p)} \propto K^2$ and $S_\Phi^{(tc)} \propto 1/K^2$ (for constant Q), one can improve the performance by increasing K until $S_\Phi^{(p)} = S_\Phi^{(tc)}$; at the same time, R_T should be made as large as possible. In the best 30 MHz-SQUIDs, the preamplifier and tank circuit noise contributions are optimized, and no significant improvement seems likely.

Another parameter that can be varied is the SQUID inductance, L. If one retains the restriction $LI_c \approx \Phi_o$, and assumes that $\alpha << 1$, one finds that α is proportional to $LI_c^{1/3}$ or to $L^{2/3}$ [Eqs. (47) and (48)]. Thus $S_\Phi^{(i)}/2L \propto L^{1/3}$, $S_\Phi^{(tc)}/2L \propto L^{4/3}$, and $S_\Phi^{(p)}/2L \propto L^0$ (since $\alpha T_N^{(p)}$ is independent of L). If $S_\Phi^{(p)}$ is the dominant noise term, no improvement is gained by reducing L. If $S_\Phi^{(tc)}$ dominates the noise, the performance can be improved by reducing L. However, a similar reduction can be achieved by increasing K, as described earlier. It should be noted that a substantial reduction in L is likely to reduce the coupling coefficient to the input coil, resulting in little overall improvement in the figure of merit. (The toroidal geometry may be an exception, since tight coupling can be achieved even with a relatively low SQUID inductance. Zimmerman's fractional-turn geometry also allows good coupling to a low inductance SQUID [72, 73].)

It is evident from Eq. (58) that all three noise contributions can be reduced by increasing ω, as is demonstrated experimentally (see Section IV-D). The use of higher frequencies appears to be the only way

to significantly improve the flux resolution. $S_\Phi^{(i)}/2L$ and $S_\Phi^{(tc)}/2L$ are both proportional to $1/\omega$, while $S_\Phi^{(p)}/2L$ is proportional to $T_N^{(p)}/\omega$ or to $S_v^{(p)}/\omega^2$. It is important to realize that as ω increases, $S_v^{(p)}$ also tends to increase, and that in practice $S_\Phi^{(p)}$ usually decreases less rapidly than $1/\omega^2$. For example, $T_N^{(p)}$ might be typically 50 K at 30 MHz and 500 K at 10 GHz. As an example, consider a SQUID with $\omega/2\pi = 10$ GHz, $\alpha = 0.2$ (this may be a low estimate at the higher frequencies), $L = 10^{-9}$ H, $T_e = 200$ K, and $T_N^{(p)} = 500$ K. We find $S_\Phi^{(i)}/2L \approx 6 \times 10^{-33}$ JHz^{-1}, $S_\Phi^{(tc)}/2L \approx 2 \times 10^{-32}$ JHz^{-1}, and $S_\Phi^{(p)}/2L \approx 10^{-31}$ JHz^{-1}. Thus the noise is dominated by preamplifier noise. This result is an order of magnitude smaller than the experimental value of Pierce et al. [78], indicating that their preamplifier had a noise temperature higher than 500 K, and, probably, that α was greater than 0.2. The use of cooled FET preamplifiers [79], which can have lower noise temperatures than room temperature preamplifiers, is a promising development. A cooled preamplifier has the added advantage of reducing T_e appreciably, so that $S_\Phi^{(tc)}$ is also reduced.

Jackel and Buhrman [40] have shown that a non-sinusoidal current-phase relation in the weak link will substantially increase the noise over that obtained with a sinusoidal current-phase relation. This result should be borne in mind when one is choosing a weak-link for use in a SQUID.

Buhrman and Jackel [private communication] have found that the ultimate energy resolution of the rf SQUID is on the order of $4 k_B T/\omega_{opt}$ where $\omega_{opt} = R/L$. Thus, the intrinsic sensitivites of the rf and dc SQUIDs with identical values of R/L are comparable. A high resistance weak link (for example, $\sim 100\ \Omega$) with a sinusoidal current-phase relation is necessary to improve the performance of both dc and rf SQUIDs. This requirement tends to favor the use of shunted tunnel junctions of small areas.

Of the various configurations of rf SQUID that have been used, the toroidal geometry has much in its favor. The device is mechanically exceedingly stable, is self-shielding against external field changes, and has a high coupling coefficient to the input coil. It would be of interest to try to incorporate a thin-film junction (for example, a shunted tunnel junction) into such a geometry.

V. SQUIDS AS MAGNETOMETERS, GRADIOMETERS, SUSCEPTOMETERS, AND VOLTMETERS

SQUIDs can be used to measure magnetic fields, magnetic field gradients, magnetic susceptibilities, and voltages. I shall describe each of these applications in turn, indicate possible future improvements, and compare the sensitivity of the SQUID-based measurement with that obtainable by other techniques. I shall begin with a description of the flux transformer, since most of the applications involve this very useful device.

A. Flux Transformer

The flux transformer consists of a superconducting loop of wire, as indicated in Fig. 22(a). The pick-up coil has N_p turns and an inductance L_p, while the input coil has an inductance L_i and a mutual inductance $M_i = \alpha (L L_i)^{1/2}$ to a flux-locked dc or rf SQUID. A magnetic field applied to the pick-up coil generates a persistent supercurrent in the flux transformer that in turn couples a flux into the SQUID. The output of the flux-locked SQUID is then proportional to the applied flux. As we shall see presently, there are a number of variations on this basic principle.

The flux resolution of the transformer is easily calculated. Suppose a magnetic field is applied to the pick-up coil so that a flux $\Delta\Phi$ threads each of the N_p turns. Flux quantization in the flux transformer requires that

$$N_p \Delta\Phi + (L_i + L_p) J = 0 \quad , \tag{59}$$

where J is the induced supercurrent. We have neglected stray inductances. The flux applied to the SQUID is then

$$\Delta\Phi_e = -M_i J = \frac{M_i N_p}{(L_i + L_p)} \Delta\Phi \quad . \tag{60}$$

We have assumed that the inductive coupling between L_i and the feedback/modulation coil is negligible (this is not necessarily true [14, 80]). If the flux noise of the SQUID (including all contributions) has a power spectrum S_Φ, the smallest flux applied to the pick-up loop that can be resolved per $\sqrt{Hz}$ is

$$\delta\Phi = \frac{L_i + L_p}{M_i N_p} S_\Phi^{1/2} = \frac{L_i + L_p}{\alpha (L_i L)^{1/2} N_p} S_\Phi^{1/2} \quad . \tag{61}$$

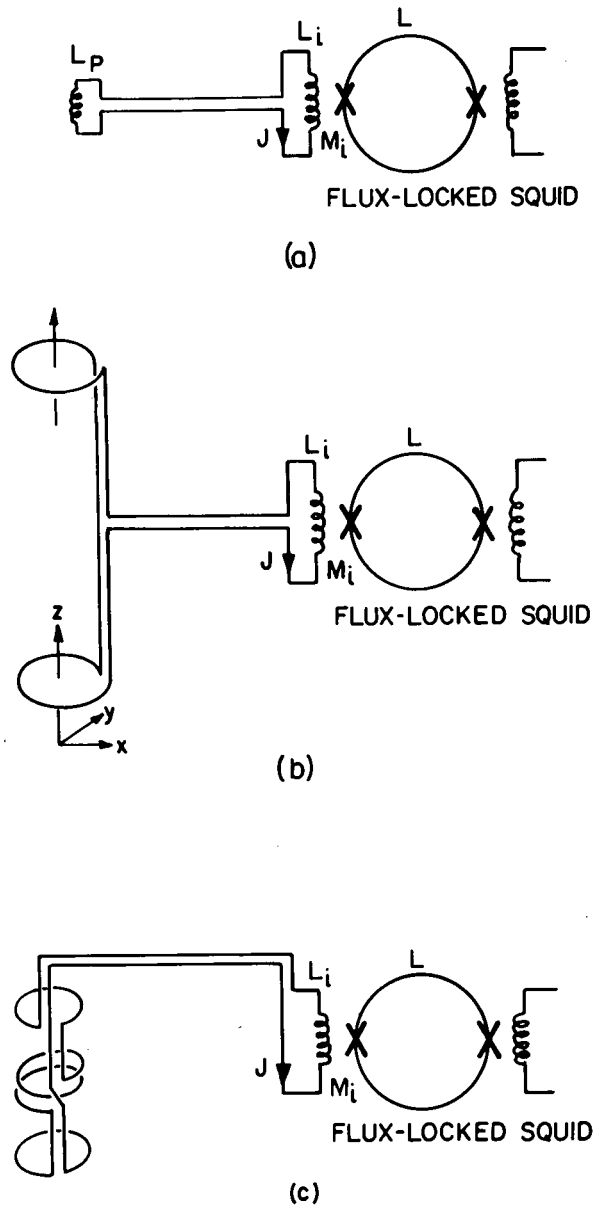

Fig. 22. (a) Flux transformer; (b) first-derivative gradiometer; and (c) second-derivative gradiometer.

For a given pick-up coil (i.e., fixed L_p and N_p), the optimum value of L_i is obtained by differentiating Eq.(61) with respect to L_i. (We assume that α remains constant as L_i is varied.) We find that $\delta\Phi$ has a minimum when $L_i = L_p$ given by

$$\delta\Phi_{min} = \frac{2L_p^{1/2}}{N_p} \left(\frac{S_\Phi}{\alpha^2 L} \right)^{1/2} . \qquad (62)$$

We notice immediately that $\delta\Phi_{min}$ is proportional to $\epsilon^{1/2}$, where ϵ is the figure of merit discussed in Section III-C, so that ϵ is an appropriate figure of merit for the flux transformer/SQUID combination.*

In the configuration just described, the flux applied to the SQUID is cancelled by a flux generated in the modulation/feedback coil. It is sometimes advantageous to couple the feedback flux into the flux transformer rather than into the SQUID. This technique has the advantage of maintaining zero supercurrent in the transformer.

I will next discuss various applications of the flux transformer.

B. Measurement of Magnetic Field

The flux-locked SQUID is of course a sensitive magnetometer for measuring changes in external magnetic field (no highly accurate method of using a SQUID to determine the absolute value of the field has yet been found). For example, the thin-film dc SQUID described in Section III-D has a magnetic field resolution of about 10^{-10} GHz$^{-1/2}$. This is a sufficiently high sensitivity for almost all practical purposes. However, it is sometimes desirable to shield the SQUID from the applied field which, if it is high enough, may cause a deterioration in the performance of the SQUID. This shielding can be achieved by placing the SQUID in a superconducting tube (for example, as shown in Fig. 10), and coupling in the field with a flux transformer. The toroidal SQUID is self-shielding against changes in external magnetic field, and a flux transformer is essential.

The pick-up coil usually has a single turn ($N_p = 1$). The smallest resolvable magnetic field change per $\sqrt{\text{Hz}}$ is then found by dividing $\delta\Phi_{min}$ by the area of the loop, A_p, so that

*Eq. (62) is not quite accurate. If a SQUID is coupled to a superconducting circuit of total inductance ℓ with a mutual inductance M_i, the effective SQUID inductance [50, 53] is lowered to a value $L' = (1 - M_i^2/L\ell)$. As a result, the voltage from the SQUID is enhanced, and the flux resolution is improved. Thus the optimization should involve L' rather than L. However, in practice, the correction is not large, and for simplicity I have ignored it.

$$\delta H_{min} = 2 \frac{L_p^{1/2}}{A_p} \left(\frac{S_\Phi}{\alpha^2 L} \right)^{1/2} . \qquad (63)$$

Since L_p varies approximately as $A_p^{1/2}$, δH_{min} is approximately proportional to $A_p^{-3/4}$. Thus, in principle, an arbitrarily high magnetic-field sensitivity can be obtained by making the pick-up loop sufficiently large, provided that the condition $L_i = L_p$ can be maintained without decreasing α. As an example, suppose the pick-up loop has a diameter of 60 mm, and an inductance of about 40 nH (40 emu). Then using $S_\Phi/\alpha^2 L \approx 1.4 \times 10^{-22}$ erg$Hz^{-1/2}$, we find $\delta H_{min} \approx 5 \times 10^{-12}$ $GHz^{-1/2}$. An increase in sensitivity of about one order of magnitude is typical.

Claassen [53] has given a more detailed discussion of coil geometries.

In a practical magnetometer, the flux transformer is almost invariably made of insulated niobium wire, typically 100 μm in diameter. It is vital that the flux transformer be rigidly attached to the SQUID, and that the pick-up loop cannot vibrate in the magnetic field. In the case of the cylindrical SQUIDs, the input coil is usually wound directly on top of the SQUID cylinder. For the dc SQUID, the coupling coefficient is about 0.6; this value appears to be typical. If the magnetometer is operated in an unshieldid environment, the pick-up loop acts as an antenna for radio and television signals, and the resultant interference coupled into the SQUID usually prevents its operation. Shielding against such interference can be obtained by surrounding the cryostat with a Faraday cage made of copper mesh. An alternative method is to place a thin-walled copper tube between the input coil and the SQUID to filter out the rf interference. The filter may introduce additional Johnson noise into the SQUID, however. The leads between the pick-up loop and the signal coil are usually twisted and surrounded by a superconducting shield. The pick-up loop is often wound on a cylinder machined on a quartz block. Three-axis magnetometers are commercially available in which the three pick-up loops are mounted on three orthogonal faces of a precision-ground quartz cube. A superinsulated fiberglass dewar (with no liquid nitrogen jacket) is frequently used. These dewars are relatively non-magnetic, readily portable, and have a boil-off rate of 1 liter or less of liquid helium per day.

These magnetometers have a higher sensitivity than can be used, at least at frequencies above (say) 1 Hz. There are no obvious applications where a sensitivity greater than 10^{-9} or 10^{-10} $GHz^{-1/2}$ is required. However, the long term drift has sometimes been higher than desirable. It appears that the drift is usually correlated with a drift in the temperature of the helium bath through changes in atmospheric pressure or the steady drop in the hydrostatic head of the liquid. These temperature changes not only cause the SQUID itself to drift, but can also cause changes in the susceptibility of the dewar, which contains paramagnetic impurities. For most applications these difficulties are

not too serious, and they can be largely removed by stabilizing the temperature of the helium bath.

The sensitivity of SQUID magnetometers is appreciably higher than that of conventional devices. The fluxgate and proton-precession magnetometers have sensitivities of about 10^{-6} $GHz^{-1/2}$, while the pumped cesium vapor magnetometer has a sensitivity of about 10^{-7} $GHz^{-1/2}$.

C. Measurement of Magnetic Field Gradient

The flux transformer may be readily adapted to measure first or even second spatial derivatives of changes in the ambient magnetic field. A gradiometer for measuring gradients of the form $\partial H_z/\partial z$ is shown schematically in Fig. 22(b). The two pick-up loops are wound so that a uniform magnetic field induces no supercurrent in the flux transformer, while a gradient $\partial H_z/\partial z$ generates a supercurrent that is proportional to the difference in the fluxes threading the two loops. Gradiometers have also been operated in which the loops are in the same plane and measure (for example) $\partial H_z/\partial x$. A straightforward analysis similar to that given in Section V-A shows that the optimum sensitivity for a given pair of coils is obtained when the inductance of the input coil, L_i, is equal to the sum of the inductances of the pick-up loops.

In a practical gradiometer, the two pick-up loops are usually wound on a precision-ground quartz block. The SQUID and the leads coupling the input coil in the gradiometer loops are shielded. It is necessary to take considerable care to ensure that the loops are as closely the same size and as accurately parallel to each other as possible. Despite these precautions, one inevitably finds that not only does the gradiometer respond to a uniform field H_z, but that it is also sensitive to fields along the x- and y-directions. It is therefore necessary to balance the gradiometer. One achieves this balance by adjusting the positions of three small pieces of superconductor along orthogonal axes by means of controls outside the cryostat. The usual procedure is to position the superconductors so as to minimize the response of the SQUID when the cryostat is rotated in the earth's field about orthogonal axes. With care, a balance of better than 1 ppm can be achieved. For two pick-up loops 6 cm in diameter and 20 cm apart, one would expect a sensitivity of better than 10^{-12} $Gcm^{-1}Hz^{-1/2}$. In practice, the sensitivity is not as high: values of 10^{-11} $G\,cm^{-1}Hz^{-1/2}$ are typical. The coupling of the gradiometer to the SQUID appears to increase the flux noise of the SQUID, for reasons that are not too well understood. The drift encountered in gradiometers is also appreciably higher than that in shielded SQUIDs by themselves. As with the magnetometers, it is believed that the drifts arise from the change in the paramagnetic susceptibility of nearly materials with changes in the temperature of the helium bath. Since the sensitivity of each pick-up loop to magnetic field changes is much higher in gradiometers than in magnetometers (which are not usually operated anywhere near their maximum possible sensitivity), the problem is much more serious in the case of gradiometers. For the

most critical low frequency applications, it is quite possible that the liquid helium dewar will have to be made from quartz (which can have a very low level of paramagnetic impurities) to reduce the drift in the gradiometer to an acceptable level.

A further development of the gradiometer is a device to measure the second derivative $\partial^2 H_z/\partial z^2$. Two first derivative gradiometers are wound end-to-end, as indicated in Fig. 22(c). Opfer et al. [68] achieved a balance against changes in a uniform magnetic field of better than 10 ppm, and against changes in magnetic field gradients of better than 1 part in 100. Brenner et al. [81] have also described a second derivative gradiometer.

There is a need for improvement in the sensitivity of gradiometers. The present gradiometers are not able to detect gradient fluctuations in the earth's magnetic field, and are therefore not limited by environmental noise (except when they are operated near machinery producing large field gradients). It is not entirely clear how such improvements can be achieved; certainly, very stringent precautions must be taken to eliminate as much paramagnetic material as possible from the helium dewar, and the whole assembly must be made extremely rigid. It also seems likely that temperature stabilization will also be required to minimize the long term drift.

In the past, all gradiometers have consisted of pickup loops coupled to a SQUID via a coil. Recently, Ketchen et al. [82] operated a thin-film gradiometer in which both the pick-up loops and the SQUID were evaporated onto a single quartz substrate. The device is sensitive to $\partial H_z/\partial x$. This configuration is extremely stable mechanically, and requires balancing only in one dimension. The device has a sensitivity of about 10^{-11} G cm^{-1} Hz$^{-1/2}$. Further development in this direction is likely.

There are no other practical devices that measure magnetic field gradients. Thus one would have to make a gradiometer by subtracting the outputs of, for example, two fluxgate magnetometers. To achieve a resolution of 10^{-11} G cm^{-1} Hz$^{-1/2}$, the magnetometers would have to be ~ 1 km apart! Clearly, one could obtain a high gradient sensitivity by placing two magnetometers far enough apart, but large separations are impracticable for many purposes. As a self-contained gradiometer, the SQUID-based system has no competition.

D. Measurement of Magnetic Susceptibility

An important application of SQUIDs is to the measurement of magnetic susceptibility. The configuration most often used is similar to that of a gradiometer, and is shown in Fig. 23. An astatic pair of niobium coils is connected to the input coil of a flux-locked SQUID. The coils are embedded in an epoxy tube that is in turn epoxied to a niobium tube, the whole assembly being extremely rigid. The sample is placed in one of the coils, as indicated. The niobium tube can be warmed above its superconducting transition temperature and cooled in an axial magnetic

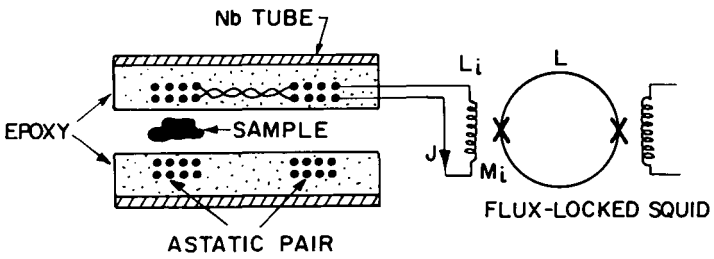

Fig. 23. Configuration used to measure magnetic susceptibility.

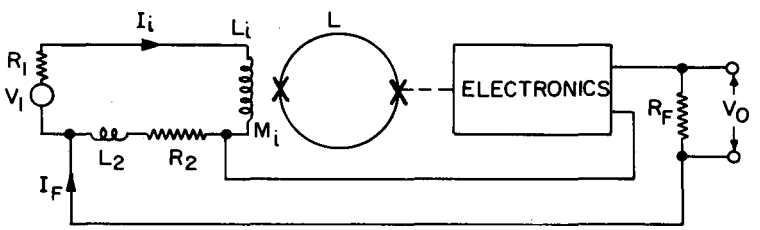

Fig. 24. Configuration of voltmeter.

field so that an exceedingly stable field is trapped (whose value, however, may differ somewhat from the applied field). If the pair of coils were perfectly balanced, the signal applied to the SQUID would be proportional to the applied magnetic field and to the magnetic susceptibility of the sample. In practice, the coils are not perfectly balanced, and it is necessary to subtract the SQUID output in the presence of the sample and sample holder from the SQUID output in the presence of the sample holder alone. (The sample holder may contribute significantly to the total susceptibility.) The temperature dependence of the susceptibility can be determined by measuring the SQUID output as a function of temperature. Again, the temperature dependence of the susceptibility of the sample holder, the epoxy, or even the enamel on the niobium wire [83,84] may be quite substantial, and it is essential to take measurements with and without the sample.

As an example, we shall quote the results obtained by Giffard et al. [9]. Let Φ be the flux applied to each turn of one of the astatic coils; Φ is thus the out-of-balance flux due to the sample. Each coil has N turns and a self-inductance $L_i/2$ (so that the astatic pair is optimally coupled to the SQUID). The flux coupled to the SQUID is then

$$\Phi_e = M_i N \Phi / 2L_i \quad . \tag{64}$$

The exact calculation of Φ is, in general, very difficult. A relatively simple limiting case [9] is when the sample consists of a small sphere, ellipsoid, or cylinder with diameter equal to height. Then

$$\Phi = 4\pi\chi HV/D \quad , \tag{65}$$

where χ and V are the susceptibility and volume of the sample, H is the trapped field, and D is the average diameter of the coils. Inserting the values [9] $N = 24$, $L_i/M_i = 166$, and $D = 3.6$ mm, we find

$$\frac{\Phi_e}{\Phi_o} = \frac{2\pi M_i N \chi H V}{L_i D \Phi_o} \approx 10^4 \chi \left(\frac{H}{1\,G}\right)\left(\frac{V}{1\,mm^3}\right). \tag{66}$$

Thus, if the resolution is limited by a SQUID noise of $10^{-4}\,\Phi_o Hz^{-1/2}$, the sensitivity in a 1 Hz bandwidth is about 10^{-7} emu for a 1 cm^3 sample in a 1 G field. Unfortunately, the resolution is usually limited by vibration and temperature drifts to a lower value.

Improvements in sensitivity have been obtained by using a larger filling factor. Cukauskas et al. [85] achieved a resolution of 10^{-10} emu for a 1 cm^3 sample in a field of 100 G, and Cerdonio and Messana [86] achieved a resolution of 6×10^{-11} emu for 0.5 cm^3 sample in a field of 200 G. A commercially available instrument [12] has a resolution of 2×10^{-11} emu for a 1 cm^3 sample in a field of 1 kG over a temperature range from 4.2 K to 400 K. The sample is rigidly suspended in a thin-walled dewar that passes through the astatic pair, and can be heated

above liquid helium temperatures. It might be noted that little increase in sensitivity results from the use of higher magnetic fields; the microphonic and/or background effects are amplified proportionately.

It seems that there is still room for improvement of SQUID-based susceptometers. The main limitations at present appear to be caused by temperature drifts that give rise to changes in the background susceptibility (see Doran and Symko [84]), and vibration of the sample in the astatic pair. It is to be hoped that both of these difficulties can be reduced, although a substantial reduction appears unlikely in the near future.

Other types of instruments have a higher sensitivity provided that one can use a higher magnetic field. Thus Foner [87] has achieved a sensitivity of 10^{-13} emu g^{-1} at 10 kG using a vibrating sample magnetometer. A commercial Faraday balance [88] has a resolution of 10^{-11} emu g^{-1} at 100 kG. These fields may, of course, be too high for some applications; at lower fields the sensitivity will be correspondingly reduced.

E. Measurement of Voltage

SQUIDs have been widely used as voltmeters, usually in the configuration of Fig. 24. The voltage source, V_1, of resistance R_1, is in series with the input coil, L_i, and a known resistance R_2 that has a stray inductance L_2. The current I_i generates a flux in the SQUID, and the electronics feeds a current $I_F = V_o/R_F$ into the resistance so that $I_F R_2 = V_1$ (in the zero frequency limit). Thus $I_i = 0$ on balance, and the voltmeter has a high input impedance. The entire voltmeter circuit and the SQUID are shielded by a superconducting can.

The dynamic behavior of the voltmeter is easily determined. We follow the treatment of Davidson et al. [52]. Let the total inductance of the voltmeter circuit be L_t, so that the time constant $\tau_T = L_t/(R_1 + R_2)$. We assume that the integration time constant in the electronics is small compared with τ_T. At a frequency ω we have

$$V_1 = I_i[R_1 + R_2 + j\omega L_t + g(R_2 + j\omega L_2)] \quad , \tag{67}$$

where $g = I_F/I_i$. If we combine Eq. (67) with

$$V_o = R_F I_F = g R_F I_i \quad , \tag{68}$$

and assume $g/(1 + R_1/R_2) \gg 0$, we obtain [52]

$$\frac{V_o}{V_1} = \frac{R_F/R_2}{1 + j\omega[(L_2/R_2) + \tau_T(1 + R_1/R_2)/g]} \quad . \tag{69}$$

At zero frequency, $V_o/V_1 = R_F/R_2$. Notice that the time constant of the loop, τ_T, is reduced by the loop gain $g(1 + R_1/R_2)$, whereas the

time constant $\tau_2 = L_2/R_2$ associated with the feedback resistor is not reduced [52].

Discussions of the noise characterization of the voltmeter have been given by several authors [9, 15, 52, 53]. The voltage noise power spectrum of the voltmeter referred to the source V_1 is just

$$S_V(\omega) = \frac{S_\Phi (R_1 + R_2)^2 (1 + \omega^2 \tau_T^2)}{M_i^2} \approx \frac{S_\Phi R_1 \left[1 + \omega^2 \tau_T^2\right]}{\alpha^2 L \tau_T} , \qquad (70)$$

if $L_t \approx L_i$, and $R_1 \gg R_2$. We then define a noise temperature [15, 49, 52, 53] $T_N(\omega)$ for the voltmeter through the relation $S_v(\omega) = 4k_B T_N(\omega) R_1$:

$$T_N(\omega) \approx \frac{S_\Phi \left[1 + \omega^2 \tau_T^2\right]}{4k_B \alpha^2 L \tau_T} . \qquad (71)$$

We notice immediately that $T_N(\omega) \propto S_\Phi / 2\alpha^2 L$, so that the figure of merit introduced in Section IV-C is also applicable to voltmeters. For low frequencies, $\omega << \tau_T^{-1}$, the noise temperature becomes independent of frequency:

$$T_N(0) \approx \frac{S_\Phi}{2\alpha^2 L} \frac{1}{2k_B \tau_T} . \qquad (72)$$

For the thin-film dc SQUID described in Section III-D, $S_\Phi / 2\alpha^2 L \approx 7 \times 10^{-30}$ JHz^{-1} in the white noise region, and $T_N(0) \approx 2.5 \times 10^{-7} \tau_T^{-1}$ K. Thus the low frequency noise temperature of a given SQUID/coil combination used as a voltmeter ultimately depends only on τ_T. In the case of the dc SQUID, the quoted figure of merit was for an input coil inductance, L_i, of about 360 nH. Thus the noise temperature, $T_N(0)$, is less than 1 K for $R_1 \leq 1.4\ \Omega$. We might expect to be able to increase L_i by at least an order of magnitude without significantly reducing α, so that an upper limit on R_1 of at least tens of ohms for a 1 K noise temperature seems perfectly feasible. If necessary, the upper limit on R_1 would be further extended by means of an additional superconducting transformer between the voltmeter circuit and the SQUID, as described by Clarke, et al. [89], and Davidson et al. [52].

For source resistances of 10Ω or less in the liquid He^4 temperature range, the resolution of SQUID voltmeters is limited by Johnson noise in the resistance. Semiconductor voltmeters [90] operated at room temperature (usually with a FET input stage) have an optimum noise temperature of about 1 K for a source impedance of about 1 M. Using a transformer cooled in the helium bath, Prober [91] has been able to couple resistances of a few ohms to a PAR 185 preamplifier and still achieve a noise temperature in the liquid He^4 temperature range.

Thus the SQUID voltmeter and the semiconductor voltmeter complement each other: the SQUID is superior for impedances below 10 Ω, while the semiconductor technology is superior for impedances above 10 Ω. A detailed discussion of the noise characteristics of the two technologies has been given by Davidson et al. [52].

IV. PRACTICAL APPLICATIONS OF SQUID-BASED DEVICES

Broadly speaking, practical applications of SQUID-based devices fall into two classes. Most applications of the magnetometer and gradiometer are "in the field", outside the laboratory, while the applications of the susceptometer and voltmeter tend to be in the laboratory. The use of SQUIDs in a non-laboratory environment has required the development of small, portable, relatively non-magnetic dewars with no nitrogen shielding and with a low boil-off rate of liquid helium. Such dewars, made of fiberglass, are now commercially available, although the paramagnetic susceptibility of the liquid helium container is too high for some applications (especially for gradiometers), and gives rise to drift when the temperature of the helium bath changes. It is hoped that this difficulty will be overcome in the near future with the aid of materials with a very low level of magnetic impurity, such as quartz.

One important use of magnetometers is in geophysics, to measure fluctuations in the earth's magnetic field. These measurements require the magnetometer to be operated at remote sites, far away from man-made magnetic disturbances. For example, W.M. Goubau, T.D. Gamble, H.F. Morrison, E.C. Mosley, and I [92] have used a three-axis SQUID magnetometer in a preliminary magnetotelluric survey in Grass Valley, Nevada. The magnetometer consists of three thin-film dc SQUIDs mounted orthogonally. The magnetotelluric technique enables one to make estimates of the electric conductivity of the earth's surface as a function of depth. Magnetic disturbance in the ionosphere and magnetosphere propagate to the earth's surface. At the earth's surface, one measures simultaneously the fluctuating components of the magnetic field (using a magnetometer) and the electric field (using electrodes buried in the ground). At a given frequency, the ratio of orthogonal components of the electric and magnetic fields is related to the conductivity of the earth's crust averaged over a skin depth at that frequency. Thus, one can estimate the conductivity as a function of depth. These techniques hold promise in surveying for geothermal sources and mineral deposits, which produce anomalies in the electric conductivity.

The short-term fluctuations in the gradient of the earth's magnetic field are probably too small to be detected by a gradiometer. However, it is possible that gradiometers may be useful for detecting relatively slow changes in the magnetization in rocks near the earth's surface. For example, there is evidence [93] that the magnetic field along a fault line changes over periods of a few days prior to an earthquake. These changes are probably due to the piezomagnetism of the rock, that is, the fact that the magnetization of the rock changes when it is stressed.

Techniques such as this might ultimately be used in earthquake prediction.

Both magnetometers and gradiometers have been used to measure magnetocardiograms and magnetoencephalograms. Much of this work has been pioneered by D. Cohen, who has recently reviewed this field [94]. Cohen, Edelsack, and Zimmerman [95] were the first to use a SQUID magnetometer to take magnetocardiograms. The signal strength was typically 5×10^{-7} G, and an elaborate screened room was necessary. Subsequently, gradiometers [67, 96, 97] have been used; because of their discrimination against signals produced by relatively distant sources, no shielding is then necessary. Second derivative gradiometers, with their even higher rejection of signals from distant sources, have been successfully applied to magnetocardiography [68, 81]. SQUIDs have also been used to obtain magnetoencephalograms [94, 98], but in this case some kind of magnetic shielding appears to be essential, as the signals are of the order of 10^{-8} G. Although both magnetocardiology and magnetoencephalography are still at the experimental stage, they offer considerable promise as routine medical techniques in the future.

A further application is to the tracking of magnetic objects. Wynn et al. [99] have used an array of three magnetometers and five gradiometers together with sophisticated processing techniques to track a moving magnetic dipole.

Susceptometers have found application in a variety of applications. One example is the investigation of electronic [100] and nuclear [9, 101, 102] magnetism in solids at ultra-low temperatures and in small magnetic fields. Mercereau and co-workers [103] have measured the susceptibility of minute biochemical samples over a temperature range from 4 to 300 K. Groups at Harvard [104] and Cornell [105] have investigated the susceptibility of small superconducting samples near their transition temperature. Yet another application is to rock magnetometry. A commercial instrument [12] is available with room temperature access that allows the susceptibility of rock samples to be quickly measured in the field.

SQUIDs and SLUGs [6] have been widely used as high resolution voltmeters. All of the measurements have been made inside superconducting shields, and have been restricted to voltages originating in the cryogenic environment. Examples include the measurement of thermoelectric emf's at low temperatures [106], of flux creep in superconductors [107, 108]; and of proximity effects in superconductor-normal metal-superconductor sandwiches [109, 110]. A SLUG was used to compare the Josephson voltage-frequency relation in different superconductors [111] to a precision of 1 part in 10^8, and to measure the quasiparticle potential in non-equilibrium superconductors [112]. Giffard et al. [9] have developed a noise thermometer in which a SQUID was used to measure the Johnson noise in a known resistor. The temperature of the resistor was deduced from the amplitude of the noise in a known bandwidth.

ACKNOWLEDGEMENTS

I am grateful to Professor R.A. Buhrman and Dr. L.D. Jackel for helpful conversations on rf SQUIDs. I should like to thank the members of the Physics Department at the University of Campinas, Brazil, for their hospitality while this article was written. This work was supported in part by the U.S. Energy Research and Development Administration.

REFERENCES

1. B.D. Josephson, Phys. Lett. 1, 251 (1962); Adv. Phys. 14, 419 (1965).
2. R.C. Jaklevic, J. Lambe, A.H. Silver, and J.E. Mercereau, Phys. Rev. Lett. 12, 159 (1964).
3. J.E. Zimmerman and A.H. Silver, Phys. Rev. 141, 367 (1966).
4. M.R. Beasley and W.W. Webb, Proc. Symp. Physics of Superconducting Devices (University of Virginia, Charlottesville, April 28-29, 1967), V. 1.
5. P.L. Forgacs and A. Warnick, Rev. Sci. Instum. 38, 214 (1967).
6. J. Clarke, Phil. Mag. 13, 115 (1966).
7. J.E. Zimmerman, P. Thiene, and J.T. Harding, J. Appl. Phys. 41, 1572 (1970).
8. J.E. Mercereau, Rev. Phys. Appl. 5, 13 (1970); M. Nisenoff, Rev. Phys. Appl. 5, 21 (1970).
9. R.P. Giffard, R.A. Webb, and J.C. Weatley, J. Low Temp. Phys. 6, 533 (1972).
10. Develco, Inc., Mountain View, CA.
11. Instruments for Technology, Helsinki, Finland.
12. S.C.T., Inc., Mountain View, CA.
13. S.H.E. Corp., San Diego, CA.
14. John Clarke, Wolfgang M. Goubau, and Mark B. Ketchen, J. Low Temp. Phys. 25, 99 (1976).
15. John Clarke, IEEE 61, 8 (1973).
16. J. Bardeen, L.N. Cooper, and J.R. Schrieffer, Phys. Rev. 108, 1175 (1957).
17. F. London, Superfluids (Wiley, NY, 1950).
18. B.S. Deaver and W.M. Fairbank, Phys. Rev. Lett. 7, 43 (1961); R. Doll and M. Näbauer, Phys. Rev. Lett. 7, 51 (1961).
19. P.W. Anderson in Lectures on the Many Body Problem, Caianiello, ed. (Academic Press. NY, 1964), Vol. 2, p. 113.
20. P.W. Anderson and J.M. Rowell, Phys. Rev. Lett. 10, 230 (1962).
21. W. Schroen, J. Appl. Phys. 39, 2671 (1968).
22. J.H. Greiner, J. Appl. Phys. 42, 5151 (1972); ibid. 45, 32 (1974).
23. J.H. Greiner, S. Basavaiah, and I. Ames, J. Vac. Sci. and Tech. 11, 81 (1974).
24. S. Basavaiah, J.M. Eldridge, and J. Matisoo, J. Appl. Phys. 45, 457 (1974).
25. J.E. Nordman, J. Appl. Phys. 40, 2111 (1969); J.E. Nordman and W.H. Keller, Phys. Lett. A36, 52 (1971); L.O. Mullen and D.B. Sullivan, J. Appl. Phys. 40, 2115 (1969); R. Graeffe and T. Wiik,

J. Appl. Phys. 42, 2146 (1971); K. Schwidtal, J. Appl. Phys. 43, 202 (1972); P.K. Hansma, J. Appl. Phys. 45, 1472 (1974); S. Owen and J.E. Nordman, IEEE Trans. Magn. MAG-11, 774 (1975).

26. R.F. Broom, R. Jaggi, R.B. Laibowitz, Th.O. Mohr, and W. Walter, Proc. LT14, Helsinki, Finland (1975), p. 172; Gilbert Hawkins and John Clarke, J. Appl. Phys. 47, 1616 (1976).
27. K.E. Drangeid, R.F. Broom, W. Jutzi, Th.O. Mohr, A. Moser and G. Sasso, Intl. Solid-State Circuits Conf. Digest, 68-69 (1971); K. Grebe, I. Ames and A. Ginzberg, J. Vac. Sci. Tech. 458 (1974).
28. W.C. Stewart, Appl. Phys. Lett. 12, 277 (1968); D.E. McCumber, J. Appl. Phys. 39, 3113 (1968).
29. P.K. Hansma, G.I. Rochlin, and J.N. Sweet, Phys. Rev. B4, 3003 (1971).
30. P.W. Anderson and A.H. Dayem, Phys. Rev. Lett. 13, 195 (1964).
31. H.A. Notarys, R.H. Wang, and J.E. Mercereau, Proc. IEEE 61, 79 (1973).
32. R.B. Laibowitz, Appl. Phys. Lett. 23, 407 (1973).
33. P. Crozat, S. Gourrier, D. Bouchon, and R. Adde, Proc. Fourteenth Intern. Conf. on Low Temperature Physics, Otaniemi, Finland, August 14-20, 1975, Matti Krusius and Matti Vuorio, eds. (North-Holland, American Elsevier, 1975), Vol. 4, p. 206.
34. F. Considori, A.A. Fife, R.F. Frindt, and S. Gygax, Appl. Phys. Lett. 18, 233 (1971).
35. M.A. Janocko, J.R. Gavaler, and C.K. Jones, IEEE Trans. Magn. MAG-11, 880 (1975); R.B. Laibowitz, C.C. Tsuei, J.C. Cuomo, J.F. Ziegler, and M. Hatzakis, ibid., p. 883.
36. J.E. Zimmerman and A.H. Silver, Phys. Rev. 141, 367 (1966).
37. J.E. Zimmerman, Proc. 1972 Applied Superconductivity Conf., Annapolis, Maryland (IEEE, NY, 1972), p. 544.
38. R.A. Buhrman, S.F. Strait, and W.W. Webb, J. Appl. Phys. 42, 4527 (1971).
39. A. Baratoff, J.A. Blackburn, and B.B. Schwartz, Phys. Rev. Lett. 25, 1096 (1970).
40. L.D. Jackel and R.A. Buhrman, J. Low Temp. Phys. 19, 201 (1975).
41. A.Th.A.M. De Waele and R.De Bruyn Ouboter, Physica 41, 225 (1969).
42. M. Tinkham Introduction to Superconductivity (McGraw-Hill, 1975), p. 214.
43. Claudia D. Tesche and John Clarke, Proceedings of the Applied Superconductivity Conference, Stanford, August 1976, in press.
44. Y.H. Ivanchenko and L.A. Zil'berman, Zh. Eksperim, I. Teor. Fiz. 55, 2395 (1968) (Sov. Phys. J.E.T.P. 28, 1272 (1969)).
45. V. Ambegaokar and B.I. Halperin, Phys. Rev. Lett. 22, 1364 (1969).
46. A.N. Vystavkin, V.N. Gubankov, L.S. Kuzmin, K.I. Likharev, V.V. Migulin, and V.K. Semenov, Phys. Rev. Appl. 9, 79 (1974).
47. C.M. Falco, W.H. Parker, S.E. Trullinger, and P.K. Hansma, Phys. Rev. B10, 1865 (1974).

48. K.K. Likharev and V.K. Semenov, J.E.T.P. Lett. 15, 442 (1972).
49. V.R. Radhakrishnan and V.L. Newhouse, J. Appl. Phys. 42, 129 (1971).
50. J.E. Zimmerman, J. Appl. Phys. 42, 4483 (1971).
51. J.M. Pierce, J.E. Opfer, and L.H. Rorden, IEEE Trans. Magn. MAG-10, 599 (1974).
52. A. Davidson, R.S. Newbower, and M.R. Beasley, Rev. Sci. Instrum. 45, 838 (1974).
53. J.H. Claassen, J. Appl. Phys. 46, 2268 (1975).
54. S.K. Decker and J.E. Mercereau, Appl. Phys. Lett. 25, 527 (1974).
55. D.W. Palmer, H.A. Notarys, and J.E. Mercereau, Appl. Phys. Lett. 25, 527 (1974).
56. W. Richter and G. Albrecht, Cryogenics 15, 148 (1975).
57. J. Clarke and Gilbert A. Hawkins, IEEE Trans. Magn. MAG-11, 724 (1975); Phys. Rev. B., October 1, 1976.
58. John Clarke and Richard F. Voss, Phys. Rev. Lett. 33, 24 (1974); Richard F. Voss and John Clarke, Phys. Rev. B13, 556 (1976).
59. W.W. Webb, IEEE Trans. Magn. MAG-8, 51 (1972).
60. See C. Kittel, Introduction to Solid State Physics (Wiley, NY, London, Sydney, Toronto, 1971), Edition IV, Appendix J.
61. P.K. Hansma, J. Appl. Phys. 44, 4191 (1973).
62. J. Kurkijärvi, Phys. Rev. B6, 832 (1972).
63. L.D. Jackel, J. Kurkijärvi, J.E. Lukens, and W.W. Webb in the 13th Intern. Conf. Low Temp. Phys., Boulder 1972 (Plenum Press, NY, 1974), Vol. 3, p. 705.
64. L.D. Jackel, W.W. Webb, J.E. Lukens, and S.S. Pei, Phys. Rev. B9, 115 (1974).
65. J. Kurkijärvi and W.W. Webb, Proc. Appl. Superconductivity Conf. Annapolis (IEEE, NY, 1972), p. 581.
66. J. Kurkijärvi, J. Appl. Phys. 44, 3729 (1973).
67. W.L. Goodman, V.W. Hesterman, L.H. Rorden, and W.S. Goree, Proc. IEEE 61, 20 (1973).
68. J.E. Opfer, Y.K. Yeo, J.M. Pierce, and L.H. Rorden, IEEE Trans. Magn. MAG-10, 536 (1974).
69. N.V. Zavaritskii and M.S. Legkostupov, Cryogenics 14, 42 (1974).
70. G.J. Ehnholm, J.K. Soini, and T. Wiik, Proc. of the Fourteenth Intern. Conf. on Low Temperature Physics, Otaniemi, Finland, August 14-20, 1975, Matti Drusius and Matti Vuorio, eds. (North-Holland/American Elsevier, 1975), Vol. 4, p. 234.
71. R. Rifkin and B.S. Deaver, Phys. Rev. B13, 3894 (1976).
72. J.E. Zimmerman, J. Appl. Phys. 42, 4483 (1971).
73. J.E. Zimmerman, Cryogenics 12, 19 (1972).
74. I am grateful to S.C.T. and S.H.E. for their collaboration in these measurements.
75. J.E. Zimmerman and N.V. Frederick, Appl. Phys. Lett. 19, 16 (1971).

76. R.A. Kamper and M.B. Simmonds, Appl. Phys. Lett. 20, 270 (1972).
77. T.D. Clark and L.D. Jackel, Rev. Sci. Instrum. 46, 1249 (1975).
78. J.M. Pierce, J.E. Opfer, and L.H. Rorden, IEEE Trans. Magn. MAG-10, 599 (1974).
79. M.R. Gaerttner, (unpublished — reported at Int. Mag. Conf., Toronto, 1974).
80. R.A. Webb, R.P. Giffard, and J.C. Wheatley, J. Low Temp. Phys. 13, 383 (1973).
81. D. Brenner, S.J. Williamson, and L. Kaufman, Proc. of the Fourteenth Intern. Conf. on Low Temp. Phys., Otaniemi, Finland, August 14-20, 1975, Matti Drusius and Matti Vuorio, eds. (North-Holland/American Elsevier, 1975), Vol. 4, p. 266.
82. Mark B. Ketchen, Wolfgang M. Goubau, John Clarke, and Gordon B. Donaldson, Proc. of the Applied Superconductivity Conf., Stanford, CA, August 17-20, 1976 (to be published).
83. E.C. Hirschkoff, O.G. Symko, and J.C. Wheatley, J. Low Temp. Phys. 4, 111 (1971).
84. J.G. Doran and O.G. Symko, IEEE Trans. Magn. MAG-10, 603 (1974).
85. E.J. Cukauskas, D.A. Vincent, and B.S. Deaver, Jr., Rev. Sci. Instrum. 45, 1 (1974).
86. M. Cerdonio and C. Messana, IEEE Trans. Magn. MAG-11, 728 (1975).
87. For recent improvements in vibrating sample magnetometers and a comprehensive bibliography see S. Foner, Rev. Sci. Instrum. 46, 1425 (1975).
88. Oxford Instruments, England.
89. J. Clarke, W.E. Tennant, and D. Woody, J. Appl. Phys. 42, 3859 (1971).
90. For example, Princeton Applied Research Model 185.
91. D.E. Prober, Rev. Sci. Instrum. 45, 848 (1974).
92. W.M. Goubau, T.D. Gamble, J. Clarke, H.F. Morrison, and E.C. Mosley (unpublished).
93. M. Johnston (private communication).
94. D. Cohen, Physics Today, August 1975, p. 34; IEEE Trans. Magn. MAG-11, 694 (1975).
95. D. Cohen, E.A. Edelsack, and J.E. Zimmerman, Appl. Phys. Lett. 16, 278 (1970).
96. J.E. Zimmerman and N.V. Frederick, Appl. Phys. Lett. 19, 16 (1971).
97. J. Ahopelto, P.J. Karp, T.E. Katila, R. Lukanda, and P. Mäkipää, Proc. of the Fourteenth Intern. Conf. on Low Temp. Phys., Matti Krusius and Matti Vuorio, eds. (North-Holland/American Elsevier, 1975), Vol. 4, p. 202.
98. D. Cohen, Science 175, 664 (1972).
99. W.M. Wynn, C.P. Frahm, P.J. Carroll, R.H. Clark, J. Wellhoner, and M.J. Wynn, IEEE Trans. Magn. MAG-11, 701 (1975).
100. E.C. Hirschkoff, O.G. Symko, and J.C. Wheatley, J. Low Temp.

Phys. 5, 155 (1971).
101. E.C. Hirschkoff, O.G. Symko, L.L. Vant-Hall, and J.C. Wheatley, J. Low Temp. Phys. 2, 653 (1970).
102. J.M. Goodkind and D.L. Stolfa, Rev. Sci. Instrum. 41, 799 (1970).
103. H.E. Hoenig, R.H. Wang, G.R. Rossman, and J.E. Mercereau, in Proceedings of the 1972 Applied Superconductivity Conference (Annapolis, Maryland) (IEEE, NY, 1972), p. 570.
104. J.P. Gollub, M.R. Beasley, R.S. Newbower, and M. Tinkham, Phys. Rev. Lett. 22, 1288 (1969).
105. J.E. Lukens, R.J. Warburton, and W.W. Webb, Phys. Rev. Lett. 25, 1180 (1970).
106. E. Rumbo, Phil. Mag. 19, 689 (1969).
107. M. Wade, Phil. Mag. 20, 1107 (1969).
108. M.R. Beasley, R. Labusch, and W.W. Webb, Phys. Rev. 181, 682 (1969).
109. J. Clarke, Proc. Roy. Soc. A308, 447 (1969).
110. A.B. Pippard, J.G. Shepherd, and D.A. Tindall, Proc. Roy. Soc. A324, 17 (1971).
111. J. Clarke, Phys. Rev. Lett. 21, 1566 (1968).
112. J. Clarke, Phys. Rev. Lett. 28, 1363 (1972); J. Clarke and J.L. Paterson, J. Low Temp. Phys. 15, 491 (1974).

PRINTED IN U.S.A.

TECHNICAL INFORMATION DIVISION
LAWRENCE BERKELEY LABORATORY
UNIVERSITY OF CALIFORNIA
BERKELEY, CALIFORNIA 94720